



UNIVERSIDADE ESTADUAL DE CAMPINAS
Faculdade de Engenharia Civil, Arquitetura e Urbanismo

THIAGO BEZERRA CORRÊA

**EFEITOS DE OCUPAÇÃO E DRAGAGEM DE
APROFUNDAMENTO NA ESTABILIDADE DA
DESEMBOCADURA DO ESTUÁRIO DE SANTOS**

**LAND RECLAMATION AND DEEPENING DREDGING
EFFECTS ON THE STABILITY OF SANTOS
ESTUARY INLET**

CAMPINAS

2018

THIAGO BEZERRA CORRÊA

**LAND RECLAMATION AND DEEPENING DREDGING
EFFECTS ON THE STABILITY OF SANTOS
ESTUARY INLET**

**EFEITOS DE OCUPAÇÃO E DRAGAGEM DE
APROFUNDAMENTO NA ESTABILIDADE DA
DESEMBOCADURA DO ESTUÁRIO DE SANTOS**

Dissertação de Mestrado apresentada à Faculdade de Engenharia Civil, Arquitetura e Urbanismo da Unicamp, para obtenção do título de Mestre em Engenharia Civil, na área de Recursos Hídricos, Energéticos e Ambientais.

Dissertation presented to the School of Civil Engineering, Architecture and Urban Design of the University of Campinas in partial fulfillment of the requirements for the degree of Master, in the area of Water Resources, Energy and Environment

Supervisor/Orientador: Prof. Dr. Tiago Zenker Gireli

ESTE EXEMPLAR CORRESPONDE À VERSÃO FINAL DA DISSERTAÇÃO DEFENDIDA PELO ALUNO THIAGO BEZERRA CORRÊA E ORIENTADO PELO PROF. DR. TIAGO ZENKER GIRELI.

ASSINATURA DO ORIENTADOR

CAMPINAS

2018

Agência(s) de fomento e nº(s) de processo(s): CAPES, 01-P-01879-2016

Ficha catalográfica
Universidade Estadual de Campinas
Biblioteca da Área de Engenharia e Arquitetura
Rose Meire da Silva - CRB 8/5974

C817L Corrêa, Thiago Bezerra, 1992-
Land reclamation and deepening dredging effects on the stability of Santos estuary inlet / Thiago Bezerra Corrêa. – Campinas, SP : [s.n.], 2018.

Orientador: Tiago Zenker Gireli.
Dissertação (mestrado) – Universidade Estadual de Campinas, Faculdade de Engenharia Civil, Arquitetura e Urbanismo.

1. Ocupações - Áreas portuárias. 2. Santos (SP). I. Gireli, Tiago Zenker, 1980-. II. Universidade Estadual de Campinas. Faculdade de Engenharia Civil, Arquitetura e Urbanismo. III. Título.

Informações para Biblioteca Digital

Título em outro idioma: Efeitos de ocupação e dragagem de aprofundamento na estabilidade da desembocadura do estuário de Santos

Palavras-chave em inglês:

Occupations - Port areas

Santos (SP)

Área de concentração: Recursos Hídricos, Energéticos e Ambientais

Titulação: Mestre em Engenharia Civil

Banca examinadora:

Tiago Zenker Gireli [Orientador]

Susana Beatriz Vinzon

Joseph Harari

Data de defesa: 30-08-2018

Programa de Pós-Graduação: Engenharia Civil

**UNIVERSIDADE ESTADUAL DE CAMPINAS
FACULDADE DE ENGENHARIA CIVIL, ARQUITETURA E
URBANISMO**

**LAND RECLAMATION AND DEEPENING DREDGING
EFFECTS ON THE STABILITY OF SANTOS ESTUARY
INLET**

Thiago Bezerra Corrêa

Dissertação de Mestrado aprovada pela Banca Examinadora, constituída por:

Prof. Dr. Tiago Zenker Gireli
Presidente e Orientador/FEC/UNICAMP

Profa. Dra. Susana Beatriz Vinzon
Universidade Federal do Rio de Janeiro

Prof. Dr. Joseph Harari
Universidade de São Paulo

A Ata da defesa com as respectivas assinaturas dos membros encontra-se no SIGA/Sistema de Fluxo de Dissertação/Tese e na Secretaria do Programa da Unidade.

Campinas, 30 de agosto de 2018.

*For Francisca Bezerra and José Corrêa
in consideration of their love, affection
and support.*

Acknowledgements

First, I thank my parents Francisca Bezerra and José Corrêa, who always provided me good opportunities to keep studying and encouraged me to follow the professional path I believe.

I acknowledge the support and inspiration given by my supervisor, Prof. Dr. Tiago Zenker Gireli, by Prof. Dr. Patricia Dalsoglio Garcia and their research team. I also thank the support of my friends from research Vinicius de Carvalho Neiva Pinheiro, Kelly Kawai Venancio, Atila Foster Klein Gunnewiek, André Lima Coelho, Camila Maria Mateus de Souza, Ana Carolina Cardoso Costa and Antonio Henrique Soares Dutra Gomes Pereira.

I also acknowledge the valuable support of all employees of School of Civil Engineering, Architecture and Urban Design, specially Eduardo Estevam and Rosana Kelly, who always provided the best conditions for postgraduate students in our school.

I appreciate the valuable contribution of the members the board Susana Beatriz Vinzon and Joseph Harari for their contribution for this work.

Also, I thank Ramboll Brazil managers Eugenio da Motta Singer and Ricardo Oliveira Camargo, who provided me conditions to balance research and environmental consultancy work.

This study was financed in part by the Coordenação de Aperfeiçoamento de Pessoal de Nível Superior - Brasil (CAPES) - 01-P-01879-2016 001.

Finally, I thank DHI for providing me a time-limited license for thesis of the Mike 21 FM software.

“The willingness to admit ignorance. Modern science is based on the Latin injunction ignoramus – ‘we do not know’. It assumes that we don’t know everything. Even more critically, it accepts that the things that we think we know could be proven wrong as we gain more knowledge. No concept, idea or theory is sacred and beyond challenge.”

Sapiens, Yuval Noah Harari

RESUMO

Durante as últimas duas décadas, os incentivos governamentais à expansão do porto levaram Santos a ser um dos principais centros de investimentos em infraestrutura. No entanto, a ocupação de terras, principalmente pela construção de terminais portuários em áreas estuarinas, afetou a estabilidade de entrada das marés do estuário de Santos. Neste trabalho, a simulação de quatro cenários utilizando modelagem hidrodinâmica aplicada auxiliou a avaliação dos efeitos derivados da ocupação de terras e da dragagem de aprofundamento na estabilidade da desembocadura do estuário de Santos entre 2006 e 2014. Revisão bibliográfica mostra que a dragagem de aprofundamento tende a aumentar prisma de maré, enquanto a ocupação de terras tende a diminuir o prisma de maré. O cenário de linha de base (2006) antecede a construção de dois terminais portuários (EMBRAPORT e BTP) e o aprofundamento da dragagem no canal de navegação do Porto de Santos. A avaliação da estabilidade na entrada do estuário de Santos consistiu em um novo método derivado da relação empírica Área-Prisma. O Método de Fatias aprimorou a precisão da estimativa da área transversal e permitiu a avaliação das alterações do perfil transversal da desembocadura do estuário. Nesse caso, o efeito da ocupação de terras se sobrepôs ao efeito da dragagem de aprofundamento e reduziu o prisma de marés do estuário de Santos. Durante esses oito anos, o prisma de maré do estuário de Santos diminuiu de $55,1 \times 10^6 \text{ m}^3$ para $53,6 \times 10^6 \text{ m}^3$, a garganta do estuário de Santos ficou mais rasa e a área da seção transversal da desembocadura reduziu 5,5%. Portanto, os efeitos cumulativos da ocupação de terra na estabilidade da desembocadura devem ser estudados para definir estratégias de mitigação do assoreamento no canal.

Palavras-chave: Ocupação de Terras, Desembocaduras, Prisma de Maré, Relação Área-Prisma, Porto de Santos.

ABSTRACT

During the past two decades, governmental incentives on port expansion have led Santos to be a hotspot of infrastructure investments. Nevertheless, land reclamation, mainly by port terminal construction in estuarine areas, has affected Santos estuary tidal inlet stability. Herein, the simulation of four scenarios using hydrodynamic modelling assisted the evaluation of the effects derived from land reclamation and deepening dredging in the stability of Santos estuary inlet between 2006 and 2014. Bibliographic review shows that deepening dredging tends to increase tidal prism, while land reclamation tends to decrease tidal prism. The baseline scenario (2006) is prior to the construction of two port terminals (EMBRAPORT and BTP) and to the deepening dredging in the navigation channel of Port of Santos. The assessment of Santos estuary inlet stability consisted of a new method derived from the empirical Area-Prism relationship. The Slice Method enhanced the cross-sectional area estimative accuracy and enabled the evaluation of inlet cross-sectional profile changes. In this case, land reclamation overlapped deepening dredging effects and reduced Santos estuary tidal prism. During these eight years, Santos estuary tidal prism decreased from $55.1 \times 10^6 \text{ m}^3$ to $53.6 \times 10^6 \text{ m}^3$, Santos estuary inlet got shallower and the cross-sectional area reduced 5.5%. Therefore, cumulative effects of land reclamation on inlet stability shall be studied to define mitigation strategies for channel siltation.

Keywords: Land Reclamation, Tidal Inlet, Tidal Prism, Area-Prism Relationship, Port of Santos.

LIST OF FIGURES

Figure 1 - Santos Estuary System composed by Santos estuary, São Vicente and Bertioga estuarine channels. Source: Adapted from Google Earth.	15
Figure 2 - Port of Santos hinterland. Source: Adapted from IPEA (2009).	18
Figure 3 - Port of Santos Dredging stretches 1 - Access Channel; 2 - from "Entrepasto de Pesca"to "Torre Grande"; 3 and 4 - from "Torre Grande"to "Alemoa".	20
Figure 4 - Location of BTP (Brazil Port Terminal) and EMBRAPORT (Brazilian Company of Port Terminals). Source: adapted from Google Earth.	21
Figure 5 - Land reclamation in Santos estuary due to EMBRAPORT construction. Source: Adapted from Google Earth.	22
Figure 6 - Construction phases 1 and 2 of port terminal BTP. Source: MKR (2008).	23
Figure 7 - Planned land reclamation in Santos estuary due to BTP construction, only phase 1 is finished. Source: MKR (2008).	23
Figure 8 - Port of Santos channel bathymetry in the Santos estuary, data from 2006 (INPH, 2007).	24
Figure 9 - Detail of Port of Santos channel bathymetry in the Santos estuary tidal inlet, data from 2006 (INPH, 2007).	25
Figure 10 - Port of Santos channel bathymetry in the Santos estuary, data from 2014 conceded by CODESP.	25
Figure 11 - Detail of Port of Santos channel bathymetry in the Santos estuary tidal inlet, data from 2014 conceded by CODESP.	26
Figure 12 - Comparison of Santos estuary tidal inlet cross-sectional area in 2006 and 2014.	26
Figure 13 - Fire Island Inlet - Great South Bay location of NOS tide prediction stations (Source: JARRETT, 1976).....	27
Figure 14 - Generic tidal inlet divided into slices.	35
Figure 15 - Representation of scatter data from several tidal inlets ($A \times P$) and from one specific tidal inlet using the Slice Method ($\Delta A \times \Delta P$).	36
Figure 16 - Model of Santos Estuary System and nearshore region 2006 bathymetry interpolated using Mike Mesh Generator.....	38
Figure 17 - Sea and riverine boundaries of the hydrodynamic model.	41
Figure 18 - Courant–Friedrichs–Lewy condition (CFL number) of Santos Estuary System and nearshore model.....	44
Figure 19 - Manning’s M bed roughness map of Santos Estuary System and nearshore model.	45
Figure 20 - Unstructured mesh of Santos Estuary System and nearshore model.	46
Figure 21 - Tide gauge stations along Santos estuary used to calibrate the hydrodynamic model. 1-Ilha das Palmas, 2-Praticagem, 3-Conceiçãozinha, 4-Ilha Barnabé and 5-Cosipa (Source: CORRÊA et al., 2018).	47
Figure 23 - Time series comparative between harmonic analysis (blue) and simulation (red) for tide gauge station (1) Ilha das Palmas, (2) Praticagem, (3) Conceiçãozinha, (4) Ilha Barnabé e (5) Cosipa (Source: CORRÊA et al., 2018).	49
Figure 23 - Time series error between harmonical analysis (OBS) and simulation (SIM) for tide gauge station (1) Ilha das Palmas (RMSE = 0.0888 m and Agreement Index = 0.9830).	51
Figure 24 - Time series error between harmonical analysis (OBS) and simulation (SIM) for tide gauge station (2) Praticagem (RMSE = 0.0444 m and Agreement Index = 0.9959).	51

Figure 25 - Time series error between harmonical analysis (OBS) and simulation (SIM) for tide gauge station (3) Conceiçãozinha (RMSE = 0.0956 m and Agreement Index = 0.9824).	52
Figure 26 - Time series error between harmonical analysis (OBS) and simulation (SIM) for tide gauge station (4) Ilha Barnabé (RMSE = 0.0698 m and Agreement Index = 0.9910).	52
Figure 27 - Time series error between harmonical analysis (OBS) and simulation (SIM) for tide gauge station (5) Cosipa (RMSE = 0.0774 m and Agreement Index = 0.9893).	53
Figure 28 - Eight flow measurement sections (S04, S05, S06, S07, S08, S09, S10, S11) along Santos estuary used to validate the hydrodynamic model for currents. ..	55
Figure 29 - Model validation for flow measurement sections S04 (a), S05 (b), S06 (c), S07 (d), S08 (e), S09 (f), S10 (g), S11 (h). Comparative between flow measurement (blue) and simulation (red).....	57
Figure 30 - Skill score for each flow station along Santos Estuary: S04=0.9366; S05=0.9360; S06=0.9279; S07=0.8362; S08=0.9001; S09=0.8431; S10=0.6165; S11=0.6427.	58
Figure 31 - AP relationship for Santos estuary tidal inlet derived from the Slice Method, and potential trend line for scatter data.	60
Figure 32 - Comparison between real and estimated cross-sectional profiles in 2014.	61

LIST OF TABLES

Table 1 - Vessel size references for Panama Canal. Source: PIANC (2014).	18
Table 2 - Port of Santos projected channel dimensions for each phase (INPH, 2007).	19
Table 3 - Classification of New Zealand estuaries (HUME AND HERDENDORF, 1988).	30
Table 4 - Empirical coefficients of AP relationship from several authors and the number of inlets used to fit the coefficients. Note: ¹ Imperial Units and ² International System	31
Table 5 - Location of the nine points in the sea boundary. Horizontal datum WGS84.	41
Table 6 - Amplitude and phase of Q1, O1, P1, K1, N2, M2, S2, K2 and M3 constituents for each point in the sea boundary.	42
Table 7 - Rivers long period discharges in the Santos Estuary System (Adapted from ROVERSI, 2012).	43
Table 8 - Maximum element area (m ²) and Manning's M roughness (m ^{1/3} /s) of Santos Estuary System hydrodynamic model according to the type of polygon.	45
Table 9 - Comparison between CHOW (1959) Manning's n roughness and Santos Estuary System hydrodynamic model Manning's n used for model calibration.	46
Table 10 - Period of tide gauge observation used in harmonical analysis of measured tidal elevation to retrieve amplitude and phase of the nine most energetic tide constituents (Q1, O1, P1, K1, N2, M2, S2, K2 and M3).	47
Table 11 - Tide gauge stations used in the model calibration, and amplitude and phase for the constituents Q1, O1, P1, K1, N2, M2, S2, K2 and M3.	48
Table 12 - Comparison between amplitude (cm) and phase (°) of nine constituents as given by Ilha das Palmas tide gauge records (FEMAR, 2000) and time series generated by hydrodynamic model.	53
Table 13 - Comparison between amplitude (cm) and phase (°) of nine constituents as given by Praticagem tide gauge records (FEMAR, 2000) and time series generated by hydrodynamic model.	54
Table 14 - Comparison between amplitude (cm) and phase (°) of nine constituents as given by Conceiçãozinha tide gauge records (FEMAR, 2000) and time series generated by hydrodynamic model.	54
Table 15 - Comparison between amplitude (cm) and phase (°) of nine constituents as given by Ilha Barnabé tide gauge records (FEMAR, 2000) and time series generated by hydrodynamic model.	54
Table 16 - Comparison between amplitude (cm) and phase (°) of nine constituents as given by Cosipa tide gauge records (FEMAR, 2000) and time series generated by hydrodynamic model.	55
Table 17 - Brief description of scenarios simulated with hydrodynamic model.	59
Table 18 – Estimates of Santos estuary tidal inlet cross-sectional area for Scenario A (baseline 2006) and Scenario D (2014).	60
Table 19 - Tidal Prism and cross-sectional area estimates for all proposed scenarios using Slice Method.	62
Table 20 - Estimative of Santos estuary tidal inlet cross-sectional area using the Area-Prism relationship with JARRETT (1976), HUGHES (2002) and HUME AND HERDENDORF (1993) coefficients.	63
Table 21 - Estimative of Santos estuary tidal inlet cross-sectional area using the Slice Method with different coefficients.	63

CONTENTS

1. INTRODUCTION.....	15
2. OBJECTIVE.....	16
3. ANTHROPOGENIC INTERVENTIONS IN SANTOS ESTUARY SYSTEM	17
3.1. From 19th Century Until Late 20th Century	17
3.2. Port of Santos Expansion in the 21st Century	17
3.2.1. Deepening Dredging	19
3.2.2. Port Terminal Expansion in Santos Estuary	21
3.2.2.1. EMBRAPORT – Brazilian Company of Port Terminals	21
3.2.2.2. BTP – Brazil Port Terminal	22
4. CHANNEL SILTATION DIAGNOSTIC	24
5. THEORETICAL FRAMEWORK.....	27
5.1. Tidal Prism.....	27
5.1.1. Tidal Prism Computation.....	27
5.1.1.1. Cubature Method	27
5.1.1.2. Integration of water discharge through inlet	28
5.1.2. Influence of Deepening Dredging in Tidal Prism.....	28
5.1.3. Influence of Basin Reduction in Tidal Prism	28
5.2. Stability of inlets	29
5.2.1. Area-Prism Relationship.....	30
5.2.1.1. Empirical Approach	30
5.2.1.2. Theoretical Approach	33
6. THE SLICE METHOD	35
6.1. Slice Method formulation	35
6.2. Calibration of Area-Prism relationship using Slice Method	37
7. HYDRODYNAMIC MODEL SETUP.....	38
7.1. Conceptual Model	38
7.2. Governing Equations	39
7.3. Data Set.....	40
7.3.1. Bathymetry	40
7.3.2. Boundary Conditions.....	41

7.3.2.1. Sea Boundaries	41
7.3.2.2. Riverine Boundaries	42
7.3.3. Numerical Stability Conditions	43
7.3.4. Mesh Definition.....	44
7.4. Model Calibration	46
7.5. Model Validation.....	55
8. STABILITY OF SANTOS ESTUARY INLET	59
8.1. Calibration of Area-Prism relationship coefficients using Slice Method	59
8.2. Validation of Area-Prism relationship using Slice Method	60
8.3. The isolated effects of land reclamation and deepening dredging.....	62
8.4. Testing different Area-Prism relationship coefficients for Slice Method	62
9. CONCLUSION	64
10. REFERENCES.....	65
I. APPENDIX.....	74
1.1. Santos estuary inlet Tidal Prism computation and cross-sectional area estimates based on coefficients $C=1.65 \times 10^{-3}$ and $q=0.81$	74
1.2. Santos estuary inlet Tidal Prism computation and cross-sectional area estimates based on JARRETT (1976), HUGHES (2002) and HUME AND HERDENDORF (1993) coefficients	76
II. ANNEX.....	78
2.1. Checklist of features that characterize each estuary type (Hume and Herdendorf, 1988).....	78
2.2. Manning's n for Channels (Chow, 1959).....	79

1. INTRODUCTION

Santos Estuary System shelters the busiest Brazilian port (Figure 1). Port of Santos importance in Brazilian history began in the late 19th century, when Coffee Cycle in São Paulo State pushed the port economically (SCAZUFCA, 2012). In 2014, it was responsible for one quarter of Brazilian balance of trade, including exports and imports of industrial and agricultural goods (CODESP, 2015).



Figure 1 - Santos Estuary System composed by Santos estuary, São Vicente and Bertioga estuarine channels. Source: Adapted from Google Earth.

Despite those benefits for Santos, major environmental impacts derive from the port. For instance, the port expansion, which mainly concerns on land reclamation, leads to basin reduction in bays or estuarine areas. This land reclamation decreases Tidal Prism (FENG *et al.*, 2015; VAN DE KREEKE, 2004), which is the amount of water entering and leaving the inlet, so it works as a flow that controls sand deposit on bars (BRUUN, 1978a). In addition, siltation increases when inlet deviates from its equilibrium. As the channel is deepened by dredging, it is harder to maintain its depth, because the relationship of depth maintenance with siltation is non-linear, following exponential or potential rate (GIRELI; VENDRAME, 2012). For those reasons, studies regarding land reclamation impacts on channel siltation are crucial to understand these processes and to mitigate this negative effect.

In the past two decades, Port of Santos has received a great deal of investments for deepening dredging, and for construction and expansion of terminals (BRASIL, 2007; BRASIL, 2013).

2. OBJECTIVE

Considering this scenario of recent anthropogenic intervention in Santos estuary, the main objective of this work is evaluating how the construction of terminals between 2006 and 2014 and the deepening dredging of Port of Santos navigation Channel affected the stability of Santos estuary inlet.

The specific objectives of this study are:

- Bibliographic review of tidal prism computation and Area-Prism relationship;
- Development of a new method to fit the coefficients of Area-Prism relationship using data from only one inlet;
- Calibration and validation of hydrodynamic model that comprises Santos Estuary, São Vicente Estuary and Bertioga Estuary.

3. ANTHROPOGENIC INTERVENTIONS IN SANTOS ESTUARY SYSTEM

3.1. From 19th Century Until Late 20th Century

Although port of Santos, in the 19th century, was a peripheral port of Portuguese America, it had natural width and depth for mooring large boats and ships at that time (MOURA, 2013).

The operationalization of São Paulo Railway in 1867 broke port logistics barriers (SCAZUFCA, 2012), and the decree signed in 1888 by Isabel, Princess Imperial of Brazil, authorized improvements in the region of port of Santos (SONDOTÉCNICA, 1977a). The combination of these measures initiated a chain of events including the construction of the first 100 meters of quay and the foundation of CDS (Santos Dock Company) (SONDOTÉCNICA, 1977a; FRF, 2008a). From the three last decades of 19th Century until the three first decades of 20th Century, Port of Santos have been economically pushed by the Coffee Cycle in São Paulo State and by the initial industrial development (SCAZUFCA, 2012). At that time, the port reached 6,259 meters of quays and moved more than 8 million tons of cargo (SONDOTÉCNICA, 1977a). According to SCAZUFCA (2012), after mid-20th Century, Port of Santos was characterized as an "Industrial Port". Indeed, the settlement of oil refineries doubled Port of Santos cargo movement (UNISANTOS *et al.*, 2014; SONDOTÉCNICA, 1977a).

Meanwhile, Port of Santos received investments for maintenance dredging (UNISANTOS *et al.*, 2014). The Access channel was 8 km long and the Navigation channel, along the estuary, was 19.5 km long (SONDOTÉCNICA, 1977a).

When the CDS concession ended, in 1980, the Federal Government created the Dock Company of the São Paulo State (CODESP) (CODESP, 2015). Later, CODESP was named Port Authority. The turning point for Port of Santos was in 1993. The Law of the Ports (Federal Law N 8630/1993) allowed Port Authorities to rent port areas to private companies (BRASIL, 1993). By this measure, Port of Santos increased its cargo handling from 28 million tons in 1990 to 42 million tons in 1999 (HILSDORF *et al.*, 2016).

3.2. Port of Santos Expansion in the 21st Century

The Law of Ports led Port of Santos to a growing pathway in container operation. Since 2003, Port of Santos is the major container operator in Latin America (FRF, 2008b), for instance investments by the port terminal "Santos Brasil" modernized and expanded the Terminal of Containers (TECON) (SANTOS BRASIL, 2011). Nevertheless, cargo movement efficiency in Port of Santos was still below the world average (FRF, 2008b).

Moreover, the Panama Canal expansion has been an important pressure for Port of Santos improvements. Panama Canal Authority (ACP) announced the Panama Canal expansion project in 2006, and the works started in the following year (ACP, 2016a). The main

purposes are the widening and deepening of existing channels, and the construction of Post Panamax dimension locks on the Pacific and Atlantic sides, also known as Third Set of Locks (URS, 2007). The expanded locks were inaugurated in 25th June 2016 (ACP, 2016b), also the new locks dimension established new vessel reference for Panama Canal, known as “Neopanamax” or “New Panamax” (Table 1).

Table 1 - Vessel size references for Panama Canal. Source: PIANC (2014).

Vessel Reference	Draught (m)	Beam (m)	Length Overall (m)
Panamax	13.2	32.2	290.0
New Panamax	15.2	49.0	366.0

Therefore, CODESP released in 2006 a Zoning Directive Plan (PDZ) aiming the expansion of Port of Santos and operation efficiency (CODESP, 2006). The plan foresaw the construction of new terminals, the deepening dredging of the Access Channel, Navigation Channel and berths, improvements in port and nearby infrastructure, and the perspective of Port of Santos assuming a role of Hub Port in South America due to its vast hinterland (Figure 2– Map of Port of Santos hinterland).



Figure 2 - Port of Santos hinterland. Source: Adapted from IPEA (2009).

3.2.1. Deepening Dredging

In response to external pressures and port bottlenecks, Brazilian Federal Government published the law N 11.610/2007 (BRASIL, 2007). This law instituted the National Dredging Program (PND 1), which aimed the deepening dredging of Brazilian ports, allowing several ports to receive larger vessels with deeper drafts (BRASIL, 2007). PND 1 summed an investment of R\$1.6 bi, and dredged about 73 million m³ of sediments from 16 ports (BRASIL, 2015).

Thus, CODESP took advantage of PND 1 investments to manage its deepening dredging. INPH (2007) projected three phases for the deepening dredging (see Table 2 with Port of Santos channel dimensions for each phase and Figure 3 with a map showing the different dredging stretches). Despite of Phase 1 accomplishment, Port of Santos is one-step behind from Panama Canal, because the Brazilian port does not support the traffic of New Panamax vessels.

Table 2 - Port of Santos projected channel dimensions for each phase (INPH, 2007).

Stretch	Extent (km)	Depth (m)			
		Before Deepening Dredging	Phase 1	Phase 2	Phase 3
1- Access Channel until "Entrepoto de Pesca"	9.5	14.0	15.0	16.0	17.0
2- From "Entrepoto de Pesca" to "Torre Grande"	4.5	13.0	15.0	16.0	17.0
3/4- From "Torre Grande" to "Alemoa"	8.5	12.0	15.0	15.0	16.0
Minimum Channel width (m)		150.0	220.0	220.0	250.0*

*Except from Ponta da Praia to Ferry-Boat (220.0 m).

In consonance with PDZ and PND 1, Port of Santos had expanded its operations by the inauguration of two important terminals, BTP (Brazil Port Terminal) and EMBRAPORT (Brazilian Company of Port Terminals) (Figure 4).

In 2013, Brazilian Federal Government published the law N 12.815/2013 (BRASIL, 2013). This law instituted the second phase of the National Dredging Program (PND 2), which aims the maintenance and deepening dredging of Brazilian ports to seek the expansion of harbor and inland navigation area. Therefore, Port of Santos is likely to set the phase 3 of dredging (Table 2), and reach the Access and Navigation channels target depth of 17 meter.



Figure 3 - Port of Santos Dredging stretches 1 - Access Channel; 2 - from "Entrepoto de Pesca" to "Torre Grande"; 3 and 4 - from "Torre Grande" to "Alemoa".

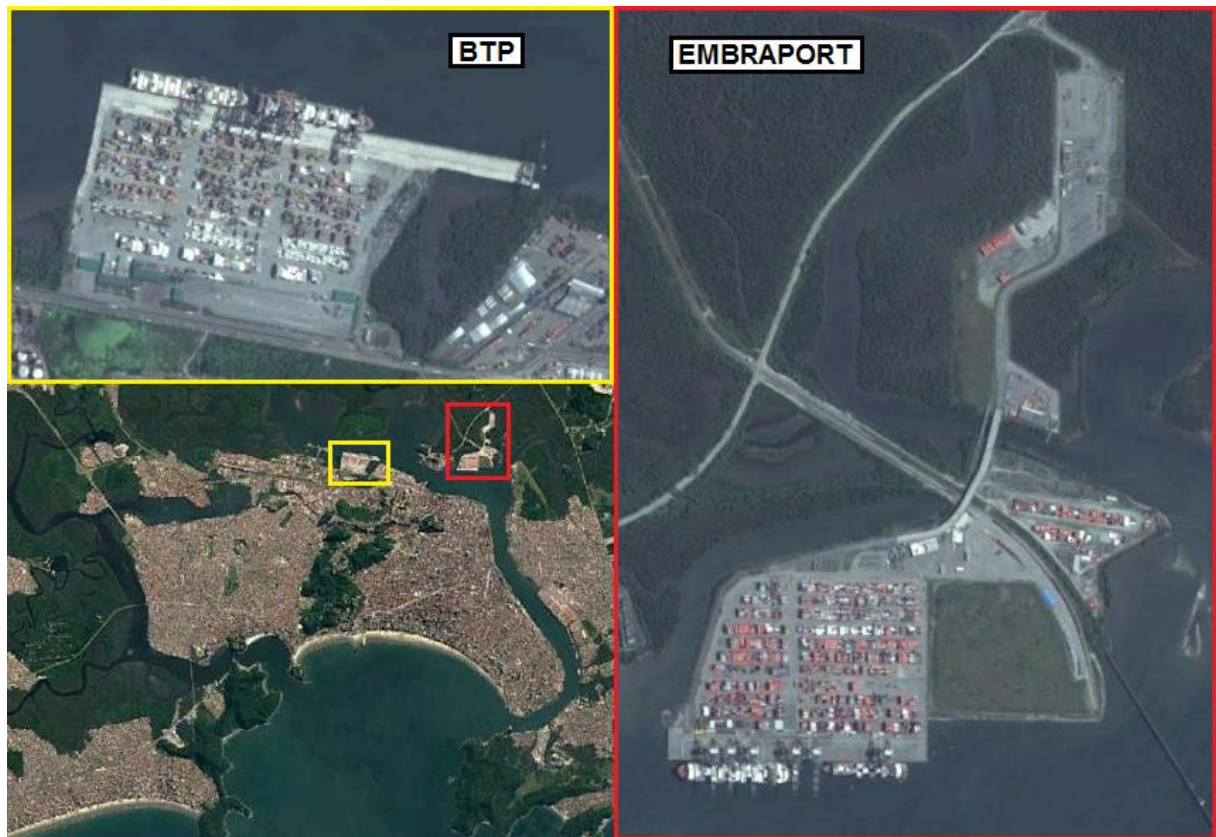


Figure 4 - Location of BTP (Brazil Port Terminal) and EMBRAPORT (Brazilian Company of Port Terminals). Source: adapted from Google Earth.

3.2.2. Port Terminal Expansion in Santos Estuary

3.2.2.1. EMBRAPORT – Brazilian Company of Port Terminals

EMBRAPORT (Brazilian Company of Port Terminals) is a private port terminal in the left margin of Port of Santos (Figure 4) with direct access to roads and railways (MKR, 2003). The terminal operations began in July 2013 (EMBRAPORT, 2013), and EMBRAPORT has an expansion planned to set an additional berth. The port terminal design follows the concept of "Beneficial Use of Dredged Material" (CPEA, 2015). This concept consists of containing dredged sediments in woven and nonwoven permeable or impermeable synthetic fabrics, such as geotextile tubes or bags, and applying them to solve construction challenges (FOWLER *et al.*, 1995).

Recently, Coastal Engineering has adopted the Beneficial Use of Dredged Material for habitat creation and enhancement (YOZZO *et al.*, 2004; BOLAM; WHOMERSLEY, 2005), access road works for bridges (CHO *et al.*, 2009), submerged shore protection (LEE; DOUGLAS, 2012; ALVAREZ *et al.*, 2007; OH; SHIN, 2006; SHIN; OH, 2007), and coastal structures (SHEEHAN; HARRINGTON, 2012).

During EMBRAPORT terminal construction, 600,000 m³ of contaminated sediments were dredged from berth and berth access, contained in 208 geotubes (2,300 m³ each), and dewatered inside three impermeable cells (WEDA, 2013). The total estimated dredged volume is 4.0 million m³, so 3.4 million m³ sediments were disposed in ocean (CPEA, 2015).

Besides, this port terminal construction resulted in phased land reclamation in the Santos estuary (Figure 5).



Figure 5 - Land reclamation in Santos estuary due to EMBRAPORT construction. Source: Adapted from Google Earth.

3.2.2.2. BTP – Brazil Port Terminal

BTP (Brazil Port Terminal) dealt with contaminated sediments too. The terminal building area used to be contaminated due to the Alemoa Dumping Ground.

Since 2007, the environmental remediation of the area demanded R\$257 mi, and eight years later CETESB (Environmental Company of São Paulo State) certified the area rehabilitation (TRIBUNA, 2015). BTP partial operations began in August 2013, the terminal turns containerized and bulk cargo (BTP, 2013).

The construction is partially concluded (Figure 6), only phase 1 is concluded. According to MKR (2008), the major land reclamation would occur when phase 2 finishes (Figure 7).

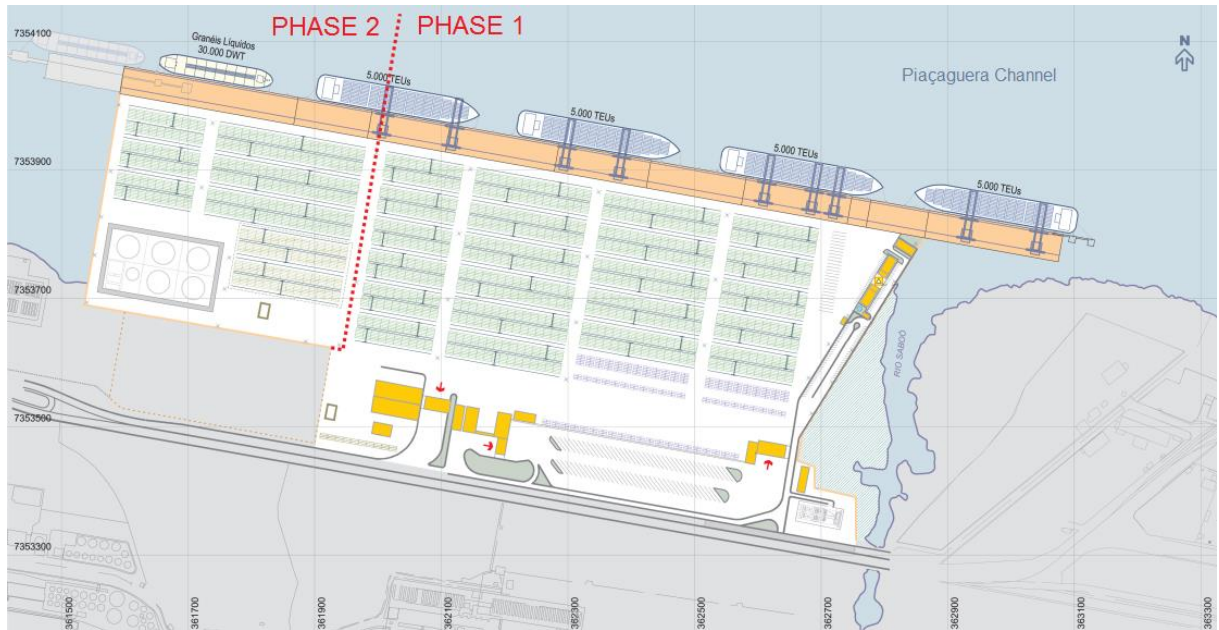


Figure 6 - Construction phases 1 and 2 of port terminal BTP. Source: MKR (2008).



Figure 7 - Planned land reclamation in Santos estuary due to BTP construction, only phase 1 is finished. Source: MKR (2008).

4. CHANNEL SILTATION DIAGNOSTIC

Port of Santos deepening dredging allowed the traffic of larger vessels, and the widening allowed the transit of two vessels, depending on their beam, side by side in the Navigation channel (see Section 3.2.1).

Figure 8 shows the surface interpolated with INPH (2007) bathymetric data from February 2006, and Figure 9 shows the detail of Santos estuary inlet before the deepening dredging. Figure 10 shows the surface interpolated with bathymetric data from October 2014, conceded by CODESP (Dock Company of the São Paulo State), and Figure 11 Figure 9 shows the detail of Santos estuary inlet after the deepening dredging.

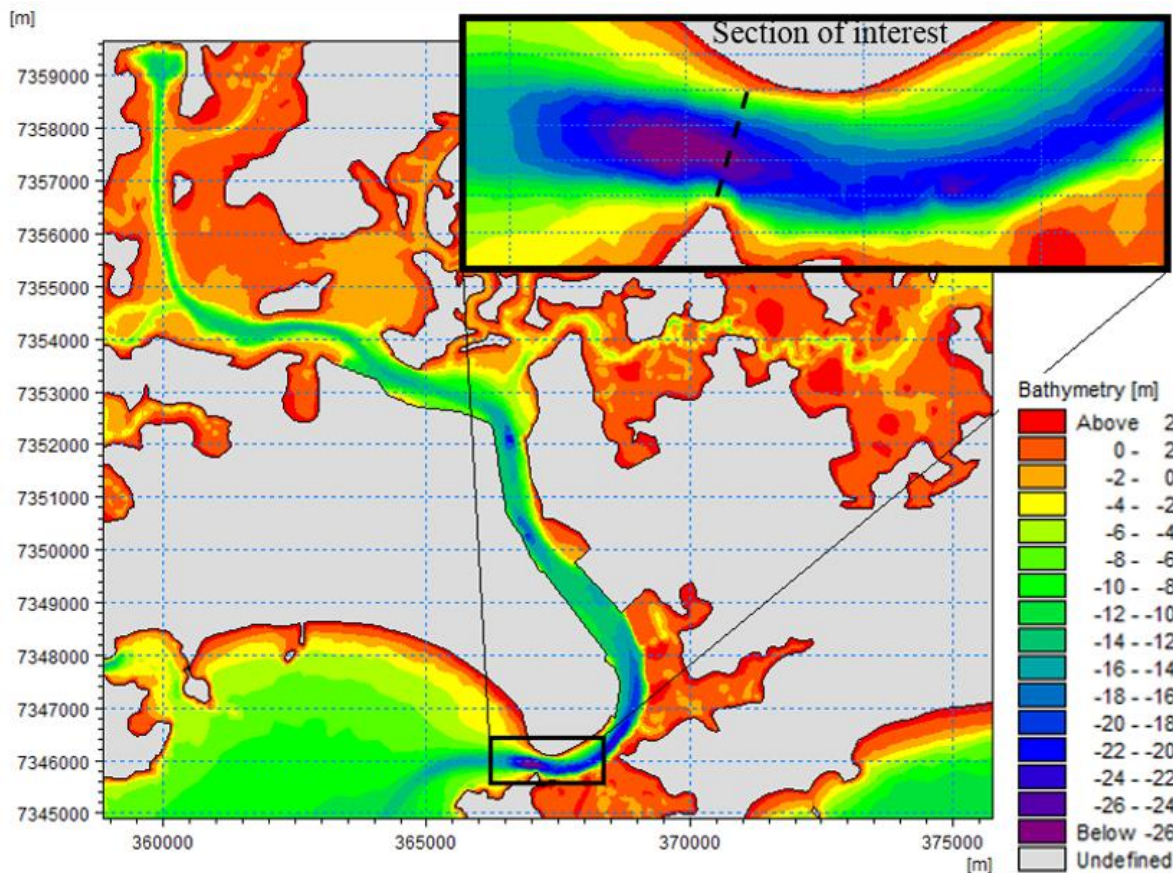


Figure 8 - Port of Santos channel bathymetry in the Santos estuary, data from 2006 (INPH, 2007).

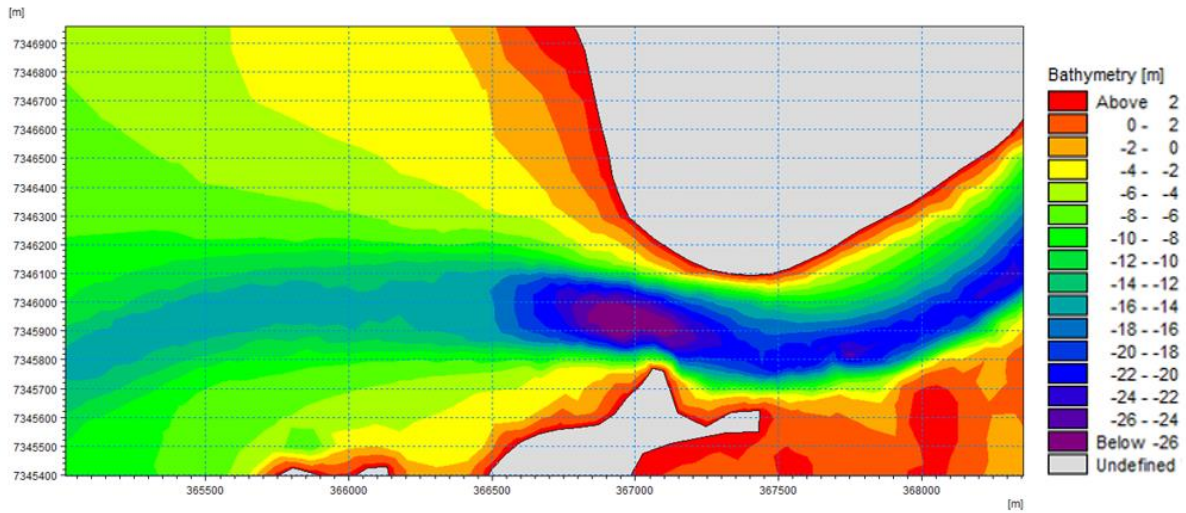


Figure 9 - Detail of Port of Santos channel bathymetry in the Santos estuary tidal inlet, data from 2006 (INPH, 2007).

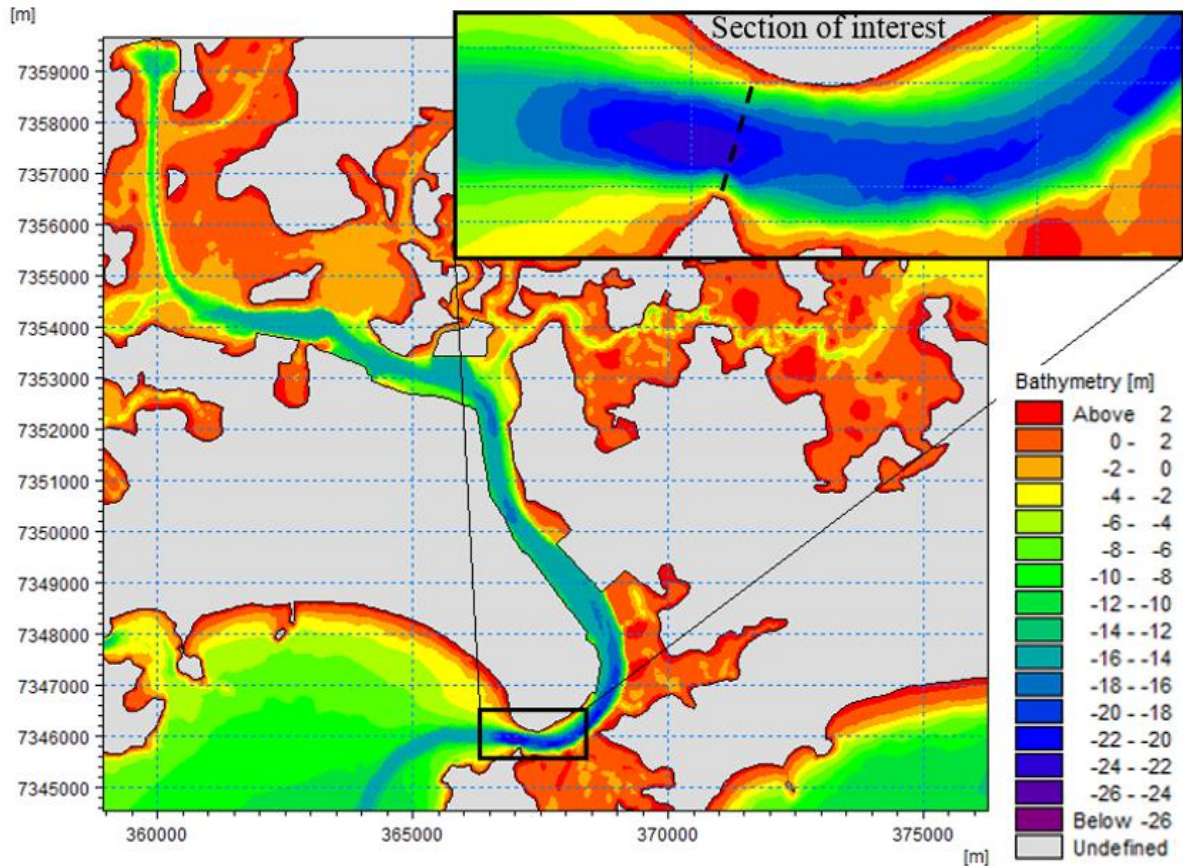


Figure 10 - Port of Santos channel bathymetry in the Santos estuary, data from 2014 conceded by CODESP.

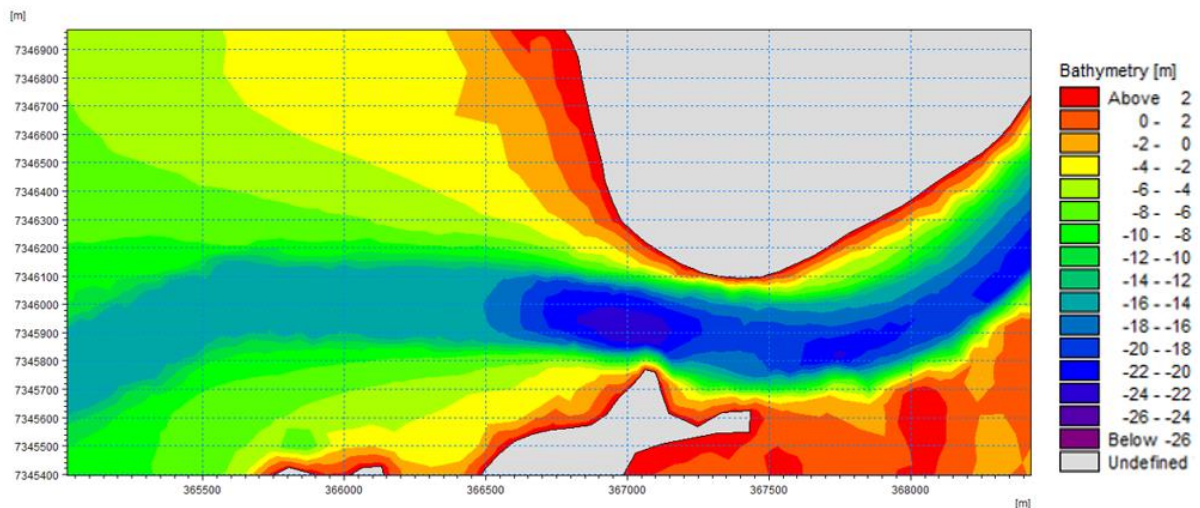


Figure 11 - Detail of Port of Santos channel bathymetry in the Santos estuary tidal inlet, data from 2014 conceded by CODESP.

Before deepening dredging, in 2006, the Port of Santos channel gorge was over 26 m deep (Figure 9). Eight years later, in 2014, the gorge got shallower and its maximum depth was under 24 m deep (Figure 11).

Indeed, Santos estuary tidal inlet got shallower (Figure 12). Its cross-sectional area reduced 5.5% in eight years, from 6,105 m² in 2006 to 5,769 m² in 2014. Considering that land reclamation decreases tidal prism (VAN DE KREEKE, 2004; FENG ET AL., 2015), understanding tidal prism variation from 2006 to 2014 and the Area-Prism relationship for Santos estuary tidal inlet is crucial to determine the synergistic effect of several estuary occupations in tidal inlet stability.

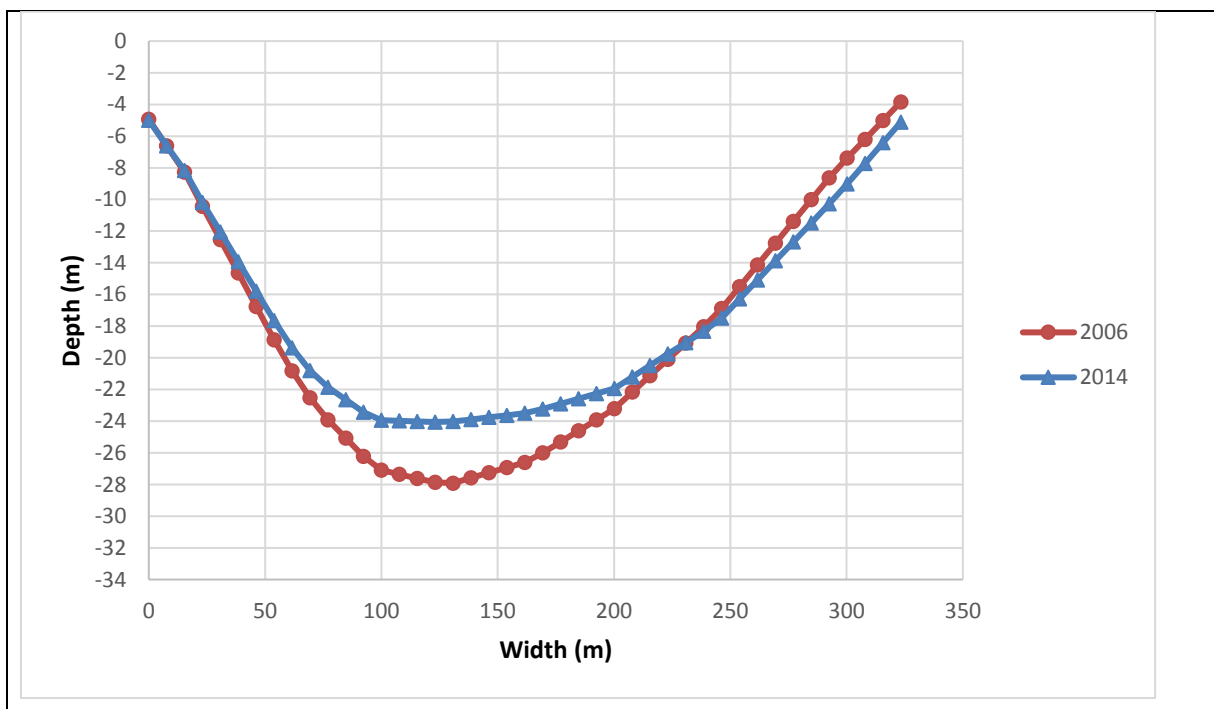


Figure 12 - Comparison of Santos estuary tidal inlet cross-sectional area in 2006 and 2014.

5. THEORETICAL FRAMEWORK

5.1. Tidal Prism

Tidal prism is the total volume of water entering or leaving the inlet (BRUUN, 1978a) and is still being used to assess tidal inlet stability, the influence in the near field waters, salinity and water renewal. Initially, tidal prism was computed as a geometrical prism. O'BRIEN (1969) describes tidal prism "as the product of the tidal area at high water slack with the diurnal or spring tidal range in the ocean at the inlet". This approach assumes a uniform variation of water elevation in tidal basins.

5.1.1. Tidal Prism Computation

5.1.1.1. Cubature Method

The tidal wave has a non-uniform propagation in the tidal basin. Thus, JARRETT (1976) proposed the Cubature Method, which takes into account the time required for tidal wave to propagate through the inlet into the bay, rather than assuming a uniform rise and fall of the tide over the entire bay (JARRETT, 1976).

Therefore, the Cubature Method segments the basin into subareas of similar "phase range". According to JARRETT (1976), phase range is "the difference between the water-surface elevation at a particular point in the bay at the time of a slack water in the inlet and the elevation at that same point at the time of a subsequent slack water in the inlet". The Tidal Prism computation consists of summing each subarea volume variation. Figure 13 shows an example of inner bay segmentation for Fire Island Inlet (JARRETT, 1976).

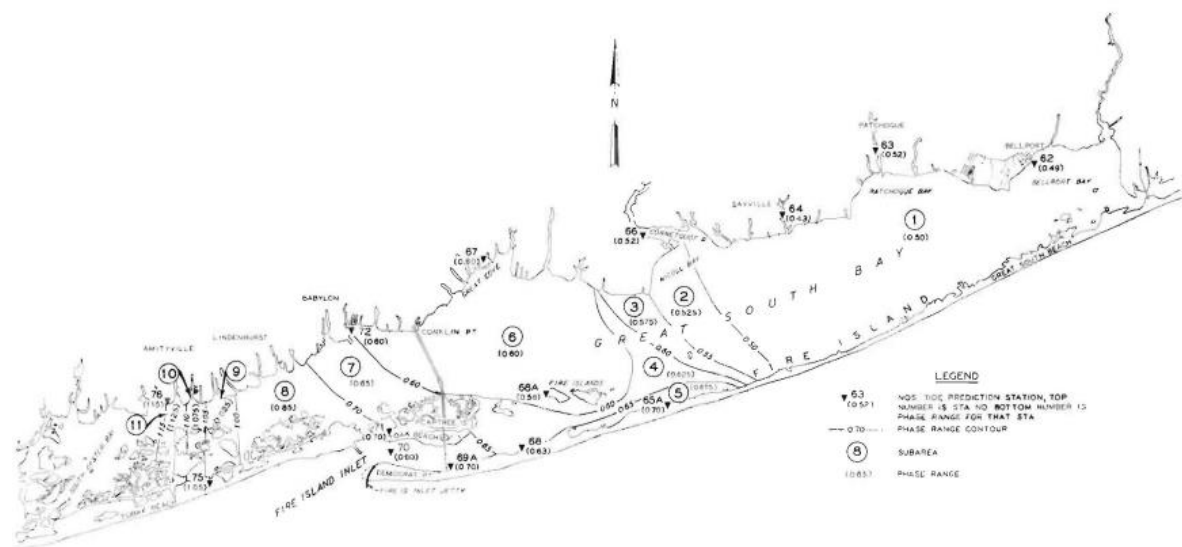


Figure 13 - Fire Island Inlet - Great South Bay location of NOS tide prediction stations (Source: JARRETT, 1976).

5.1.1.2. Integration of water discharge through inlet

Going further on tidal prism definition, it is the volume of water that enters into the bay between low slack water and the next high slack water (flood prism), or the volume of water that leaves the inlet between high slack water and the next low slack water (ebb prism) (MEHTA; ÖZSOY, 1978).

Moreover, differences in hydraulic boundary conditions such as freshwater discharge, tidal asymmetry, and the presence of multiple inlet in bay system, cause a difference between ebb and flood tidal prism volume, also known as skewness (BRUUN, 1978b). Therefore, the most reliable way of tidal prism (P) computation is the integral of water discharge ($Q(t)$) through the inlet during ebb or flood period (T) (Equation 1).

$$P = \int_0^T Q(t)dt \quad \text{Equation 1}$$

As shown in Chapter 3, the major anthropogenic changes in Santos estuary from 2006 to 2014 were land reclamation, or basin reduction, and deepening dredging. The influence of land reclamation and dredging in estuaries have been studied worldwide in several inlets.

5.1.2. Influence of Deepening Dredging in Tidal Prism

In general, several studies suggest that deepening dredging increases tidal prism, since tidal propagation in estuaries and lagoons depends on bathymetry and channel geometry. Thus, dredging the channel and relocating the inlet may increase tidal amplitude, and hence tidal prism (OLIVEIRA *et al.*, 2006; MALHADAS *et al.*, 2009; PICADO *et al.*, 2010). Indeed, when shallow channels with fair stable inlets have their bathymetry deepened, the tidal prism increases, and the inlet equilibrium cross-sectional area enlarges (CLEARY; FITZGERALD, 2003; MALHADAS *et al.*, 2009). However, in multiple inlet bay system, the enlargement of cross-sectional area of one inlet may decrease the stability of adjacent inlets (CLEARY; FITZGERALD, 2003; VAN DE KREEKE, 1990a; VAN DE KREEKE, 1990b).

The effects of dredging depends on artificial maintenance of the depth (OLIVEIRA *et al.*, 2006). An over deepened channel have stronger siltation (WAL *et al.*, 2002). FRIEDRICHS (1995) says that deepening dredging may decrease the peak velocity, so the channel may have accelerated siltation or even return to the equilibrium cross-sectional area. For instance, the urban estuarine harbor of Norfolk, Virginia, after deepening dredging, presented a sedimentation rate 90 times higher than the expected rate (NICHOLS; HOWARD-STROBEL, 1991).

5.1.3. Influence of Basin Reduction in Tidal Prism

Management of tidal basin area is fundamental for tidal inlet stability. Several studies point out that anthropogenic intervention by occupying or diking tidal flats, mangroves,

marshes or lagoons reduce tidal prism. According to CHAUMILLON *et al.* (2004), tidal prism reduction implies tidal currents decrease, which results in deposition of finer sediments.

Artificial closure of portion of bays, estuaries and lagoons by diking or damming causes sudden decrease in tidal prism. Thus, tidal inlet may take more than one decade to reach a new equilibrium (KREEKE, 2004; OOST, 1995) or even develop new barrier islands (WILLIAMS *et al.*, 2013). Dispersed occupation, such as paddy fields (AMANO *et al.*, 2006) and oyster farms (BERTIN *et al.*, 2005), also reduces tidal prism.

Likewise, construction of port terminals and harbor facilities in estuaries, bays and lagoons reduces tidal prism (FENG *et al.*, 2015; CUVILLIEZ *et al.*, 2009; WAL *et al.*, 2002; LIRIA *et al.*, 2009; SHI *et al.*, 2011). The succession of constructions, mainly on embankments, leads to cumulative effect of multiple land reclamation (CUVILLIEZ *et al.*, 2009; FENG *et al.*, 2015). Also, an appropriate management of dredged sediments is important, infilling intertidal zones modifies current velocities in the estuary and reduces tidal prism (LIRIA *et al.*, 2009; NICHOLS; HOWARD-STROBEL, 1991).

Moreover, the combination of artificial closure, successive construction of port facilities, and urban land reclamation produce a synergistic effect that reduces tidal prism and accelerate sedimentation. Several studies from China agree with this conclusion (FENG *et al.*, 2015; LIU *et al.*, 2012; SHI *et al.*, 2011; DAI *et al.*, 2016; GONG *et al.*, 2009; WANG *et al.*, 2013; WANG *et al.*, 2014).

5.2. Stability of inlets

Tidal inlets are entrances, usually shaped by tidal currents, which connect lagoons, estuaries and tidal basins to the ocean. During ebb and flood, tidal currents exchange water and sediments along the tidal channel that may interact with littoral drift and waves.

BRUUN (1978a) classifies inlets into three groups according to their origins:

- Geological origin: inlets with rocky gorges, which do not follow the alluvial inlets behaviour;
- Hydrological origin: inlets formed where river meets the ocean. The penetration of tidal currents in river mouth is the major forcing to shape the inlet geometry; and
- Littoral drift origin: in lets that might migrate in the direction of resultant littoral drift, their major forcing are waves and tidal currents.

HUME AND HERDENDORF (1988) classified New Zealand's inlets into five classes, according to their primary process that shaped the basin forming the estuary. The five classes are divided into 16 types (Table 3).

Table 3 - Classification of New Zealand estuaries (HUME AND HERDENDORF, 1988).

Primary origin of depositional basin	Estuary type		
Fluvial erosion	Funnel-Shaped (Type 1)		
	Headland enclosed (Type 2)		
	Barrier enclosed	Double-spit (Type 3)	
		Single-spit (Type 4)	
		Tombolo (Type 5)	
		Island (Type 6)	
		Beach (Type 7)	
	River mouth	Straight-banked (Type 8)	
		Spit-lagoon (Type (Type 9)	
		Spit-lagoon 2 (Type 10)	
		Deltaic (Type 11)	
Marine/fluvial	Coastal embayment (Type 12)		
Tectonism	Fault defined embayment (Type 13)		
	Diastrophic embayment (Type 14)		
Volcanism	Volcanic embayment (Type 15)		
Glaciation	Glacial embayment (Type 16)		

5.2.1. Area-Prism Relationship

Worldwide, investigators (JARRETT, 1976; O'BRIEN, 1969; HUME AND HERDENDORF, 1993; TOWNEND, 2005; POWELL et al., 2006) observed that inlets with large cross-sectional area were associated to large basins (lagoons, estuaries, coastal embayments etc.). The combination of basin surface area with tidal range lead to a volume of water in the basin stored during flood or released during ebb.

Thus, the Area-Prism relationship (AP relationship) derives from that empirical observation. Equation 2 shows the AP relationship, where A (m^2) is the tidal inlet equilibrium cross-sectional area, P (m^3) is the spring tidal prism, and C and q are coefficients of adjustment. Thus, tidal prism has been acknowledged as an indicator of tidal inlet stability.

$$A = CP^q \quad \text{Equation 2}$$

5.2.1.1. Empirical Approach

For several tidal inlets, investigators measured cross-sectional area, computed tidal prism, and plotted those data to determine coefficients that best fit the equation for scatter data. For instance, in the USA, some authors (O'BRIEN, 1969; JARRETT, 1976) grouped tidal inlets according to their locations, and/or whether the entrance was single or double jettied.

O'BRIEN (1969) observed the tidal prism of diurnal tide and minimum flow area at entrances of 28 inlets of Atlantic coast, Pacific coast and Gulf of Mexico, of the total amount 8 were without jetty, 3 with one jetty, and 17 with two jetties. Table 4 shows the AP relationship (Equation 2) fit for these scatter data.

JARRETT (1976) reanalyzed O'Brien's data and completed his comprehensive investigation by gathering and computing the Spring or Diurnal Tidal Prism and the cross-

sectional area of 162 inlets: 79 in Atlantic coast, 36 in Gulf of Mexico and 47 in Pacific coast, which were subdivided into unjettied or single-jettied (96 inlets), and double-jettied inlets (66 inlets). These data divided into these groups and subdivided into subgroups led to 11 AP relationships (Table 4).

DIECKMANN et al. (1988) investigated 37 inlets along German Bight, between Den Helder in the Netherlands and Skallingen in Denmark, where the coast is a typical barrier island-inlet region. This study consisted of collecting data concerning on tidal heights (at MHW – mean high water, MLW – mean low water and HTWL – half-tide water level), cross-sectional area of the inlet (at MHW, MLW and HTWL) and mean tidal prism (computed using tidal height and drainage basin hypsometric curves). Table 4 shows the AP relationship (Equation 2) fit for these scatter data.

Another approach is grouping the inlets according to physical features of the estuary where the inlet is located in. HUME AND HERDENDORF (1988) classified New Zealand's estuaries into five classes, divided into 16 types based on a checklist (ANNEX 2.1). Then, HUME AND HERDENDORF (1993) defined the AP relationship empirical coefficients for nine estuary types (Table 4).

TOWNEND (2005) gathered information on 66 inlets from United Kingdom regarding tidal prism and cross-sectional area at mean tide level. Then, classified these inlets in terms of geographical location, isostatic movement, tidal range, estuary type, and estuary length. One of the main findings of this study was that the AP relationship in UK estuaries shows a dependence on estuary length.

POWELL et al. (2006) compiled data from 28 inlets from Atlantic coast and 39 from Gulf coast in Florida, and defined morphodynamic relationships between tidal prism, inlet throat area, and ebb and flood delta volumes. Table 4 shows the AP relationship (Equation 2) fit for these scatter data.

Table 4 - Empirical coefficients of AP relationship from several authors and the number of inlets used to fit the coefficients. Note: ¹Imperial Units and ²International System

Parameter (country)	C	q	# of inlets	Source
All inlets (US) ¹	4.69×10^{-4}	0.85	28	O'Brien (1969)
All inlets (US) ¹	5.74×10^{-5}	0.95	162	Jarrett (1976)
Atlantic Coast (US) ¹	7.75×10^{-6}	1.05	79	Jarrett (1976)
Gulf Coast (US) ¹	5.02×10^{-4}	0.84	36	Jarrett (1976)
Pacific Coast (US) ¹	1.19×10^{-4}	0.91	47	Jarrett (1976)
No or one Jetty – all inlets (US) ¹	1.04×10^{-5}	1.03	96	Jarrett (1976)
No or one Jetty – Atlantic Coast (US) ¹	5.37×10^{-6}	1.07	50	Jarrett (1976)
No or one Jetty – Gulf Coast (US) ¹	3.51×10^{-4}	0.86	30	Jarrett (1976)
No or one Jetty – Pacific Coast (US) ¹	1.91×10^{-6}	1.10	16	Jarrett (1976)
Two Jetties – all inlets (US) ¹	3.76×10^{-4}	0.86	66	Jarrett (1976)
Two Jetties – Atlantic Coast (US) ¹	5.77×10^{-5}	0.95	29	Jarrett (1976)
Two Jetties – Gulf Coast (US) ¹	Insufficient data for regression analysis		6	Jarrett (1976)

Parameter (country)	C	q	# of inlets	Source
Two Jetties – Pacific Coast (US) ¹	5.26×10^{-4}	0.85	31	Jarrett (1976)
German Bight (Germany) ²	3.72×10^{-4}	0.915	37	Dieckmann et al. (1988)
Funnel-shaped (New Zealand) ²	4.21×10^{-2}	0.719	4	Hume and Herdendorf (1993)
Headland enclosed (New Zealand) ²	7.02×10^{-5}	1.054	5	Hume and Herdendorf (1993)
Barrier enclosed (New Zealand) ²	2.46×10^{-4}	0.927	32	Hume and Herdendorf (1993)
River mouth (New Zealand) ²	4.39×10^{-3}	0.757	5	Hume and Herdendorf (1993)
Coastal embayment (New Zealand) ²	5.46	0.529	4	Hume and Herdendorf (1993)
Tectonic-fault (New Zealand) ²	2.54×10^{-2}	0.778	9	Hume and Herdendorf (1993)
Tectonic-diastraphic (New Zealand) ²	1.48×10^{-2}	0.989	4	Hume and Herdendorf (1993)
Fiord (New Zealand) ²	9.50×10^{-5}	1.165	6	Hume and Herdendorf (1993)
Auckland inlets (New Zealand) ²	6.54×10^{-5}	1.027	11	Hume and Herdendorf (1993)
Atlantic and Gulf coasts (US) ²	6.25×10^{-5}	1	67	Powell et al. (2006)

A brief analysis of AP relationship empirical coefficients (Table 4) points out that coefficients fitted to inlets from several locations and without any sort of filter (e.g. All inlets US) presents different values of C and q, depending on the inlets considered. O'BRIEN (1969) and JARRETT (1976) defined general equations for "All inlets (US)", considering Pacific, Atlantic and Gulf coasts. Despite the coefficient q were close, the coefficient C is very different. Since, the first fitted its curve with 28 points and the latter with 162 points, the composition of the scatter data may be composed by different proportions of locations. POWELL et al. (2006), investigated 28 inlets from Florida (Atlantic and Gulf coasts), and its AP relationship coefficients were similar to JARRETT (1976) coefficients for "All inlets (US)" (162 inlets) and for "Two Jetties – Atlantic Coast (US)" (29 inlets). The first similarity might be a coincidence, but the second may have some points in coincidence, since the group of inlets have similar locations.

Moreover, the presence of jetties influences the AP relationship. Some patterns may be found when comparing JARRETT (1976) general coefficients for Atlantic, Pacific and Gulf coasts (general groups) with JARRETT (1976) coefficients for Atlantic, Pacific and Gulf coasts filtered by "no or one jetty" and "two jetties". These groups of inlets filtered by "no or one jetty" subgroups have lower values for C for the three locations, which means that these inlets need more tidal prism to maintain large cross-sectional area. Also, the subgroups of inlets with "two

jetties” have higher values of C for the three locations, which means that these inlets need less tidal prism to maintain large cross-sectional area.

The analysis of DIECKMANN ET AL. (1988) and HUME AND HERDENDORF (1993) figures shows that empirical coefficients depend more on estuary’s physical attributes than on inlets’ location. DIECKMANN ET AL. (1988) analyzed 37 inlets in German Bight, where most inlets are barrier islands. HUME AND HERDENDORF (1993) barrier enclosed inlets group (Types 3 to 7, Table 3) are built from sand supply by onshore transport of shelf sand and/or littoral drift (HUME AND HERDENDORF, 1988). Since both groups show similar physical attributes, their coefficients are similar too.

Later, STIVE et al. (2010) re-scrutinized existing data (JARRETT, 1976; POWELL et al., 2006), categorizing those inlets according to their mean grain size, tidal range, hydraulic radius, and littoral transport. Despite the high correlations between the stable inlet predicted by each AP relationship and the corresponding data, only in a limited number of categories were the correlations significantly better than the correlations for the complete datasets (STIVE et al., 2010). That may occur because the curve fit need a large number of inlets to determine good empirical coefficients.

5.2.1.2. Theoretical Approach

KRAUS (1998) proposed the first theoretical approach for AP relationship, which accounts the dynamic balance between inlet ebb tidal transport and longshore sand transport. However, this method leads to larger predicted cross-section area when the littoral transport is low.

HUGHES (2002) developed a theoretical AP relationship (Equation 3), which derives from the assumption that the maximum discharge per unit width through an inlet is at equilibrium with every depth across the minimum cross section. This formulation is based on a critical shear stress for noncohesive sediments.

In Equation 3, coefficient C depends on tidal period (T), median grain size (d_e), channel width (W), gravity (g), sediment specific gravity (S), and a coefficient related to the effects of non-sinusoidal tides (k_a). This formulation was validated with data from 102 inlets (US) and results from 18 small-scale movable bed models.

$$A = 0.65 k_a \left[\frac{W^{\frac{1}{9}}}{[g(S-1)]^{\frac{4}{9}} d_e^{\frac{1}{3}} T^{\frac{8}{9}}} \right] P^{8/9} \quad \text{Equation 3}$$

TOWNEND (2005) tested HUGHES (2002) formulation (Equation 3) for UK inlets and found that this formulation is a good predictor. Since the estimated cross-sectional areas were

similar to measured values, TOWNEND (2005) concluded that this formulation (Equation 3) should be further developed to properly reflect cohesive and noncohesive environments.

Moreover, according to HUGHES (2002), the coefficient C is strongly influenced by tidal period, with sediment mean grain size and inlet width having only minor influence.

6. THE SLICE METHOD

A brief bibliographic review on Area-Prism relationship (section 5.2.1) shows that the equation accuracy depends most on two factors to fit the coefficients C and q , the quantity of inlets and the similarity between these inlets.

Considering HUGHES (2002) assumption that the maximum discharge per unit width through an inlet is at equilibrium with every depth across the minimum cross section, a new approach of Area-Prism relationship curve fitting is proposed. Instead of considering the entire inlet cross section and its corresponding tidal prism from several locations, this method consists of picking the inlet of one location, slicing it into several pieces and computing the partial tidal prism, the contribution of each slice of the cross-sectional area for the tidal prism volume. Therefore, this method, henceforth referred as Slice Method, seeks to determine the Area-Prism relationship for a specific location and the cross-sectional profile of the tidal inlet of interest. In order to achieve that, some considerations are required.

6.1. Slice Method formulation

The analytical discharge integration to calculate tidal prism (Equation 1) can be written in discrete form (Equation 4), where Δt is the length of time step, i is the time step, t is the number time steps, and Q_i is the discharge in a given time step.

$$P = \sum_{i=1}^t Q_i \Delta t \quad \text{Equation 4}$$

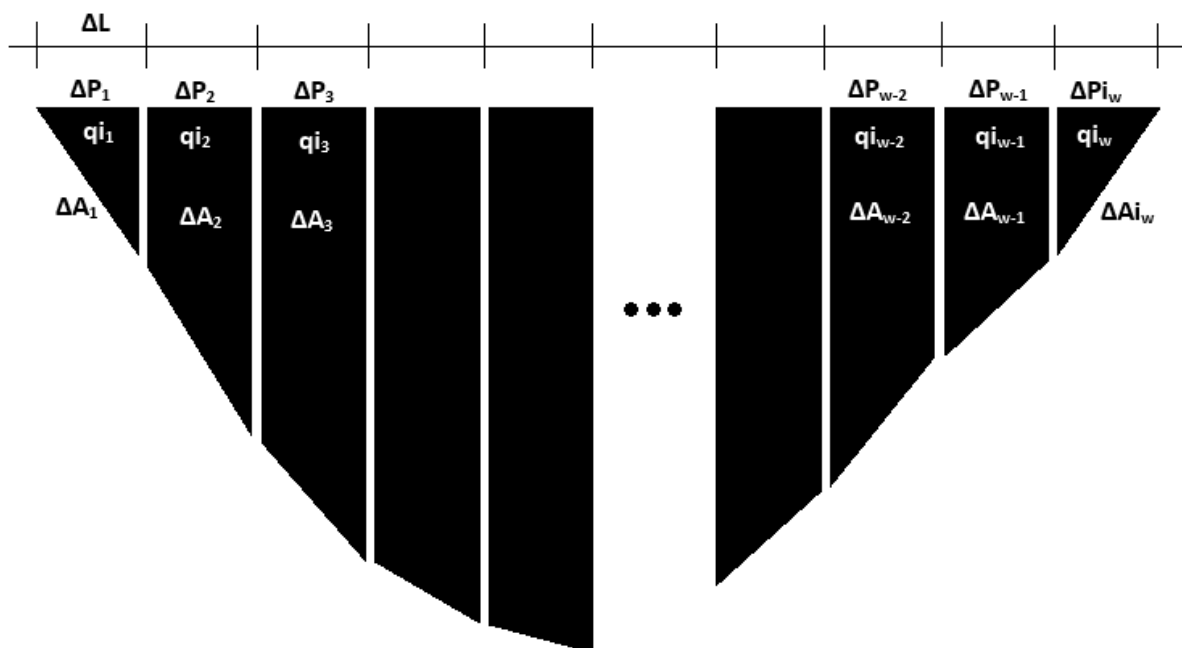


Figure 14 - Generic tidal inlet divided into slices.

Considering the cross-sectional area divided into several slices with equal width (Δl) (Equation 4 and Figure 14), during one time step i the discharge Q_i can be divided into several specific discharges q_{ij} (Equation 5).

$$Q_i = \sum_{j=1}^w q_{ij} \Delta l \quad \text{Equation 5}$$

Combining Equation 4 and Equation 5, Equation 6 represents tidal prism discretized in time and space.

$$P = \sum_{i=1}^t \sum_{j=1}^w q_{ij} \Delta l \Delta t \quad \text{Equation 6}$$

Considering only one slice j , the integration of its specific discharge (q_{ij}) in time provides a volume of partial tidal prism, hereafter called slice tidal prism (ΔP) (Equation 7). The sum of all w slice tidal prisms (ΔP_j) results in the tidal prism (P) (Equation 8).

$$\Delta P_j = \sum_{i=1}^t q_{ij} \Delta l \Delta t \quad \text{Equation 7}$$

$$P = \sum_{j=1}^w \Delta P_j \quad \text{Equation 8}$$

Instead of defining the coefficients C and q from scatter data of area (A) versus tidal prism (P) from several inlets, the Slice Method uses each slice area (ΔA) and slice tidal prism (ΔP) from a unique tidal inlet (Figure 15). Furthermore, when the slice width (Δl) is small enough, the slice area (ΔA) divided by the slice width (Δl) may be a fair approximation for the depth of each point along the cross-section. Then, the Slice Method may provide the tidal inlet cross-sectional profile.

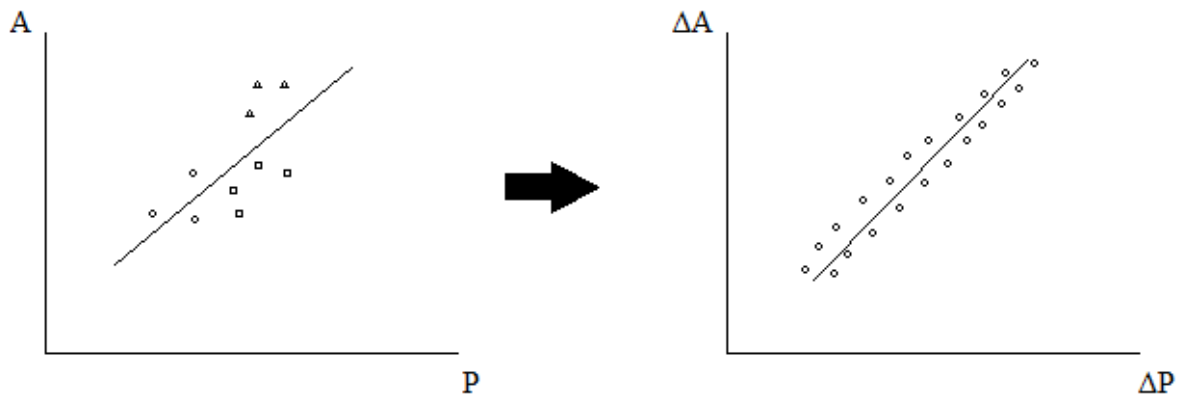


Figure 15 - Representation of scatter data from several tidal inlets ($A \times P$) and from one specific tidal inlet using the Slice Method ($\Delta A \times \Delta P$).

The only issue for this method is the difficulty to measure the specific discharge for several slices along tidal inlet cross-section on the field. Depending on the inlet width and/or on the traffic of vessels through the inlet, the measurements may be unfeasible. Nevertheless, the time series for specific discharge along tidal inlet can be retrieved from a hydrodynamic numerical model calibrated and validated for astronomical tides and currents.

6.2. Calibration of Area-Prism relationship using Slice Method

The calibration of coefficients C and q is based on a non-linear optimization model. The model consists of calculating the differences between measured (ΔA_j) and computed ($\overline{\Delta A_j}$) area for each slice, and then minimizing the sum of the square of these differences (Equation 9). The Generalized Reduced Gradient method solves the optimization model.

$$\text{Min Error} = \sum_{j=1}^w (\Delta A_j - \overline{\Delta A_j})^2 \quad \text{Equation 9}$$

It is important to emphasize that this adjustment works better for interpolations. Therefore, the Slice Method may be applied using Equation 10, so the total cross-sectional area will be the sum of all slices (Equation 11).

$$\Delta A_j = C (\Delta P_j)^q \quad \text{Equation 10}$$

$$A = \sum_{j=1}^w \Delta A_j = \sum_{j=1}^w C (\Delta P_j)^q \quad \text{Equation 11}$$

7. HYDRODYNAMIC MODEL SETUP

7.1. Conceptual Model

According to (SONDOTÉCNICA, 1977a; SONDOTÉCNICA, 1977b), the hydraulics in the Santos Estuary System depends mainly on tidal propagation, and salinity induces an internal circulation that changes vertical velocity profiles.

Thus, considering the main objective of this study, only astronomical tide effects were considered in the hydrodynamic model. Santos tides have diurnal inequalities, so this region presents mixed tide (FRANCO, 1988), and in estuarine areas tides are influenced by river discharges (HARARI and CAMARGO, 2003).

Therefore, using the available tide gauge stations (Figure 21) and flow measurements (Figure 28) this hydrodynamic model intends to reproduce tidal currents along Santos Estuary System.

In addition, the estuary geometry also influences the hydraulics (SONDOTÉCNICA, 1977a; SONDOTÉCNICA, 1977b; LEITÃO et al., 2008; ROVERSI, 2012), so changes in the estuary bathymetry due to deepening dredging and land reclamation are important factors (CORRÊA et al., 2016).

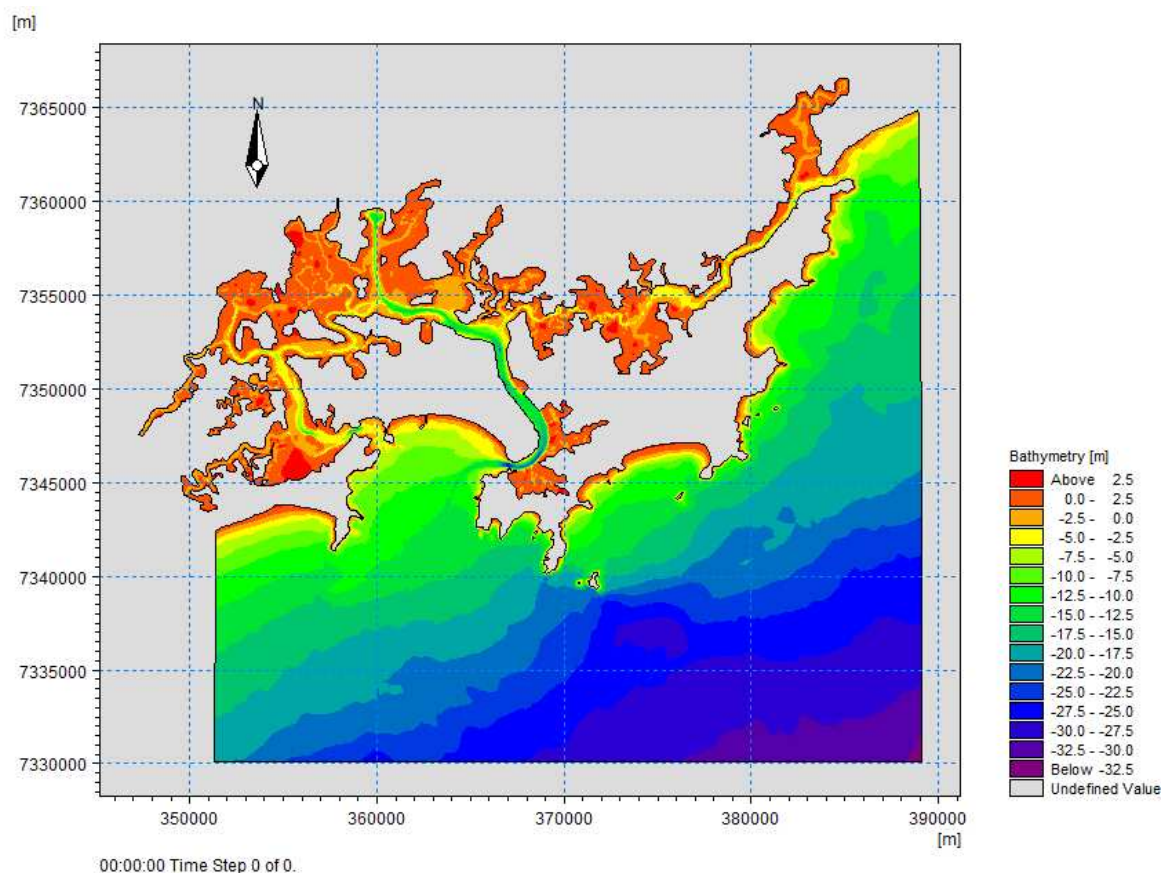


Figure 16 - Model of Santos Estuary System and nearshore region 2006 bathymetry interpolated using Mike Mesh Generator.

Three channels, São Vicente Estuary, Port of Santos (Santos Estuary) and Bertioga Estuary, form Santos Estuary System (Figure 16), where meanders, channel ramifications and mangrove inundation areas influence the hydraulics in the estuary.

Since the main forcing in the region is astronomical tide, tidal currents and water elevation are the main phenomena to assess the influence of land reclamation and deepening dredging on the stability of Santos Estuary inlet.

7.2. Governing Equations

The current study applies a 2D hydrodynamic model with flexible mesh (Mike 21 Flow Model FM). This hydrodynamic module solves two-dimensional shallow water equations (the depth-integrated incompressible Reynolds averaged Navier-Stokes equations), the spatial discretization of equations is performed using a cell-centered finite volume method, and in the horizontal plane, an unstructured grid is adopted comprising of triangles or quadrilateral elements (DHI, 2015).

As seen in section 7.1, the area of interest is mainly estuarine, where the main hydrodynamic forcing is the sea level variation on sea boundaries. Thus, for the proposed study, a simple model with continuity and momentum equations are enough to reach the study purposes. The model consists on one continuity Equation 12 and two horizontal momentum equations, Equation 13 for x coordinate and Equation 14 for y coordinate. The 2D module uses depth-averaged velocities U and V, and performs an explicit scheme for the time integration (DHI, 2015).

$$\frac{\partial h}{\partial t} + \frac{\partial hU}{\partial x} + \frac{\partial hV}{\partial y} = hS \quad \text{Equation 12}$$

$$\begin{aligned} \frac{\partial hU}{\partial t} + U \frac{\partial U}{\partial x} + V \frac{\partial U}{\partial y} & \quad \text{Equation 13} \\ & = fVh - gh \frac{\partial \eta}{\partial x} - \frac{gh^2}{2\rho_0} \frac{\partial \rho}{\partial x} - \frac{1}{\rho_0} \left(\frac{\partial S_{xx}}{\partial x} + \frac{\partial S_{yy}}{\partial y} \right) + \frac{\partial}{\partial x} (hT_{xx}) \\ & \quad + \frac{\partial}{\partial y} (hT_{xy}) + hu_s S \end{aligned}$$

$$\begin{aligned} \frac{\partial hV}{\partial t} + U \frac{\partial V}{\partial x} + V \frac{\partial V}{\partial y} & \quad \text{Equation 14} \\ & = -fUh - gh \frac{\partial \eta}{\partial y} - \frac{gh^2}{2\rho_0} \frac{\partial \rho}{\partial y} - \frac{1}{\rho_0} \left(\frac{\partial S_{yx}}{\partial x} + \frac{\partial S_{yy}}{\partial y} \right) + \frac{\partial}{\partial x} (hT_{xy}) \\ & \quad + \frac{\partial}{\partial y} (hT_{yy}) + hv_s S \end{aligned}$$

Where t is the time; x and y are the Cartesian coordinates; η is the surface elevation; d is the still water depth; $h = \eta + d$ is the total water depth; U and V are the Earth velocity components in the x and y direction; $f = 2\Omega \sin\phi$ is the Coriolis parameter (Ω is the angular rate of evolution and ϕ is the geographic latitude); g is the gravitational acceleration; ρ is the density of water; s_{xx} , s_{xy} , s_{yy} and s_{yx} are components of the radiation stress tensor; ν_t is the vertical turbulent (or eddy) viscosity; ρ_0 is the reference density of water. S is the magnitude of the discharge due to point sources and (u_s, v_s) is the velocity by which the water is discharged into the ambient water. The lateral T_{ij} include viscous friction, turbulent friction and differential advection. They are estimated using an eddy viscosity formulation based on the depth averaged velocity gradients (Equation 15).

$$T_{xx} = 2A \frac{\partial U}{\partial x}; T_{xy} = A \left(\frac{\partial U}{\partial y} + \frac{\partial V}{\partial x} \right); T_{yy} = 2A \frac{\partial V}{\partial y} \quad \text{Equation 15}$$

7.3. Data Set

7.3.1. Bathymetry

The baseline of this study is set for 2006, thus the Port of Santos Access and Navigation Channel are retrieved from bathymetric data of this year based on INPH (2007) survey.

Parts of the estuary are from older surveys (MARMIL, 2015; GARCIA *et al.*, 2002) or are interpolated values (SOUZA, 2017), and the nearshore area and some parts of the estuary are retrieved from nautical charts and DHN bathymetric data, which the scatter data comprises data from 1969 to 2004 (MARMIL, 2015; GARCIA *et al.*, 2002):

- DHN bathymetric data:
 - FB – 1700-005/82 – From ‘Ilha da Moela’ to ‘Ilha Montão de Trigo’ – scale 1:100000 (GARCIA *et al.*, 2002);
- Nautical Charts:
 - Chart n. 1701 (detail of São Vicente) – scale 1:23000 (MARMIL, 2015);
 - Chart n. 1711 (Port of Santos vicinity) – scale 1:80000 (MARMIL, 2015);
- Hydrographic surveys:
 - CTH – 1976 - São Vicente Bay and Estuary – scale 1:2000 (GARCIA *et al.*, 2002);
 - INPH – 2006 – Access Channel to Port of Santos – scale 1:5000 (INPH, 2007); and
 - Mangrove (estimative) - Floodplains and parts of Bertioga channel were estimated using hydrographic surveys interpolation and Google Earth images (SOUZA, 2017).

7.3.2. Boundary Conditions

7.3.2.1. Sea Boundaries

In accordance with the Conceptual Model 7.2, the major model forcing is tidal elevation in open sea boundary. This boundary consists of nine nodes (Table 5) and eight segments (Figure 17), which are interpolation between two consecutive points in this boundary.

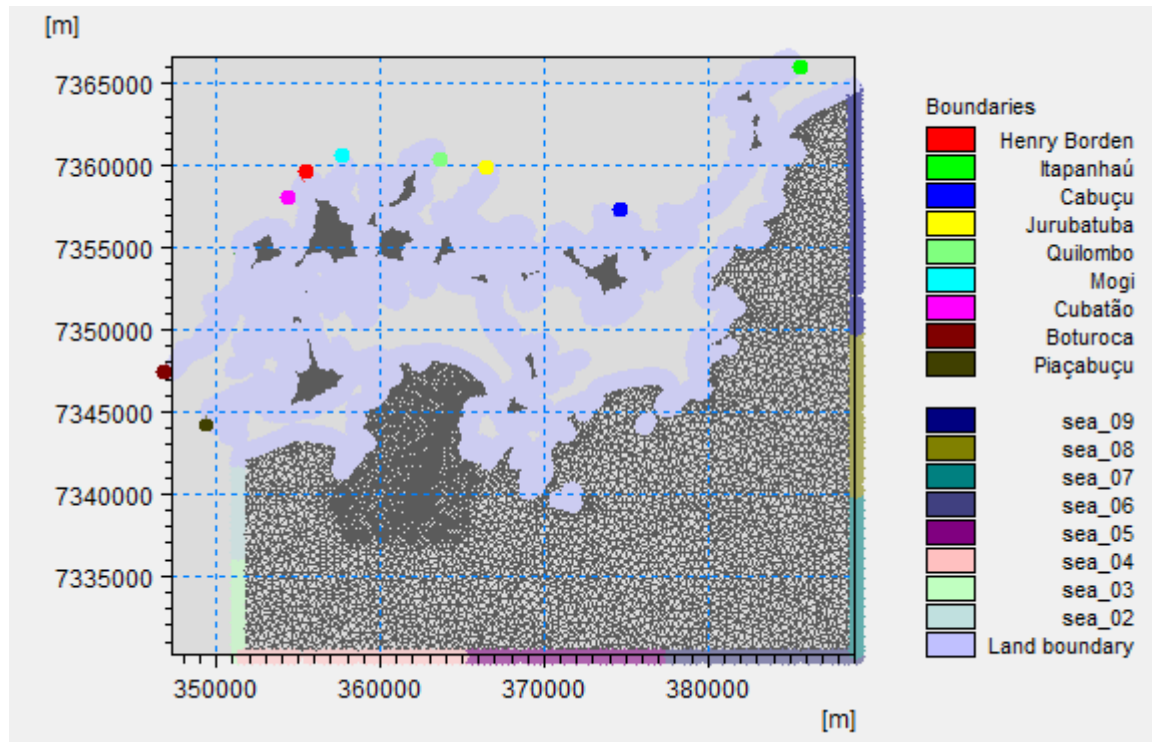


Figure 17 - Sea and riverine boundaries of the hydrodynamic model.

Table 5 - Location of the nine points in the sea boundary. Horizontal datum WGS84.

Points	East (m)	North (m)
P01	351,351.5	7,341,574.5
P02	351,351.5	7,335,707.4
P03	351,295.5	7,330,092.4
P04	365,280.0	7,330,092.4
P05	377,113.0	7,330,092.4
P06	389,067.2	7,330,101.8
P07	389,067.2	7,339,662.1
P08	389,067.2	7,349,706.8
P09	389,067.2	7,364,742.8

HARARI and CAMARGO (1994) simulated the nine most energetic tidal constituents separately in the southeastern Brazilian Shelf and draw cotidal charts of amplitude and phase for each constituent. Later HARARI and CAMARGO (2003) made detailed simulations of the coastal region of Santos, with high-resolution model. These cotidal charts allow the extraction of amplitude and phase in any point of Santos coastal area, and even predicting tidal elevations and tidal currents in the region (HARARI and CAMARGO, 1994).

GUNNEWIEK et al. (2017) generated TIN (Triangular Irregular Network) surfaces based on cotidal charts for Santos region (HARARI and CAMARGO, 1994) for amplitude and phase of constituents Q1, O1, P1, K1, N2, M2, S2, K2 and M3. According to HARARI and CAMARGO (1994), these constituents are responsible for more than 90% of tidal effects in the region.

Using GUNNEWIEK et al. (2017) surfaces as interpolation for cotidal charts, the amplitude and phase difference between the nine boundary points (Table 5) were retrieved for each constituent. Point P06 was the reference point, and it was assumed that the constituents in this point had the same amplitude and phase of Ilha da Moela constituents (using FEMAR, 2000 as reference). Finally, these amplitude and phase differences were summed to P06 tidal constituents in order to determine the other nodes tidal constituents. Table 6 shows amplitude and phase of constituents Q1, O1, P1, K1, N2, M2, S2, K2 and M3 in the time zone UTC +0 (Coordinated Universal Time).

Table 6 - Amplitude and phase of Q1, O1, P1, K1, N2, M2, S2, K2 and M3 constituents for each point in the sea boundary.

Point	A/Ph	K1	K2	M2	M3	N2	O1	P1	Q1	S2
P01	(m)	0.0907	0.0663	0.3453	0.0525	0.0327	0.1158	0.0291	0.0460	0.2413
	(°)	178.56	170.24	162.29	313.72	205.87	114.27	179.73	97.65	170.01
P02	(m)	0.0906	0.0663	0.3421	0.0533	0.0326	0.1157	0.0291	0.0460	0.2413
	(°)	178.56	169.85	162.02	313.16	205.33	114.20	179.43	97.48	169.80
P03	(m)	0.0907	0.0660	0.3409	0.0536	0.0323	0.1153	0.0291	0.0470	0.2406
	(°)	178.56	169.51	161.75	312.69	205.16	114.12	179.01	97.24	169.59
P04	(m)	0.0879	0.0644	0.3332	0.0487	0.0311	0.1151	0.0285	0.0470	0.2356
	(°)	178.45	169.04	161.06	312.95	204.48	114.11	178.34	97.62	169.00
P05	(m)	0.0860	0.0630	0.3260	0.0450	0.0300	0.1150	0.0280	0.0470	0.2310
	(°)	177.93	168.57	160.58	313.04	203.84	114.09	177.68	97.80	168.41
P06	(m)	0.0842	0.0617	0.3187	0.0413	0.0289	0.1149	0.0276	0.0470	0.2270
	(°)	177.00	168.00	160.00	313.00	203.00	114.00	177.00	98.00	168.00
P07	(m)	0.0841	0.0622	0.3204	0.0418	0.0294	0.1156	0.0276	0.0470	0.2288
	(°)	178.16	168.37	160.24	314.10	203.34	114.20	177.68	98.24	168.30
P08	(m)	0.0839	0.0628	0.3220	0.0423	0.0298	0.1163	0.0276	0.0460	0.2304
	(°)	178.56	168.74	160.62	315.25	203.67	114.41	178.32	98.51	168.73
P09	(m)	0.0838	0.0637	0.3232	0.0424	0.0306	0.1173	0.0275	0.0460	0.2322
	(°)	178.56	169.55	160.26	316.63	204.14	115.19	178.52	98.76	169.32

7.3.2.2. Riverine Boundaries

The hydrodynamic model has nine points of river discharge along the estuary (Figure 17), Table 7 shows the long period discharges in the Santos Estuary System (ROVERSI, 2012).

Table 7 - Rivers long period discharges in the Santos Estuary System (Adapted from ROVERSI, 2012).

River	Discharge (m ³ /s)
Boturoca	7.18
Cabuçu	3.43
Cubatão	8.09
Itapanhaú and Itatinga	20.28
Jurubatuba	3.91
Mogi	3.58
Piabuçu	2.27
Quilombo	4.55
Henry Borden	6.00

The base line is from 2006 and the foreseen scenario is from 2014, two scenarios eight years apart. Thus, the study does not account changes in river discharge regime, which are constant in time.

7.3.3. Numerical Stability Conditions

Before retrieving results from a numerical model, it is necessary to check consistency, stability and convergence conditions (HARARI, 2015). First, the finite difference equations and differential equations must be consistent, that is, spatial increments (Δx and Δy) must be as close as possible to zero, then the finite difference equation will be similar to differential equation. Second, finite difference equation solution must be stable, so spurious errors will not increase during simulation. Third, the convergence between solutions of finite difference equation and differential equation. According to the Lax Equivalence Theorem, convergence is guaranteed when consistency and stability are checked (HARARI, 2015).

The 2D DHI models have two methods of time integration, the low order method and the higher order method (DHI, 2015). The principal parts of Equation 12, Equation 13 and Equation 14 are advection related terms, so an explicit, time centered and spatial centered (higher order) discretization method is conditionally stable and does not consume computation resources as an implicit method (HARARI, 2015).

The stability is checked using the Courant–Friedrichs–Lewy condition (CFL number) (COURANT et al., 1967). The CFL number Equation 16 for flow modelling (HARARI, 2015; DHI, 2015) must be between -1 and 1 to guarantee stability.

$$CFL = (\sqrt{gh} + |u|) \frac{\Delta t}{\Delta x} + (\sqrt{gh} + |v|) \frac{\Delta t}{\Delta y} \quad \text{Equation 16}$$

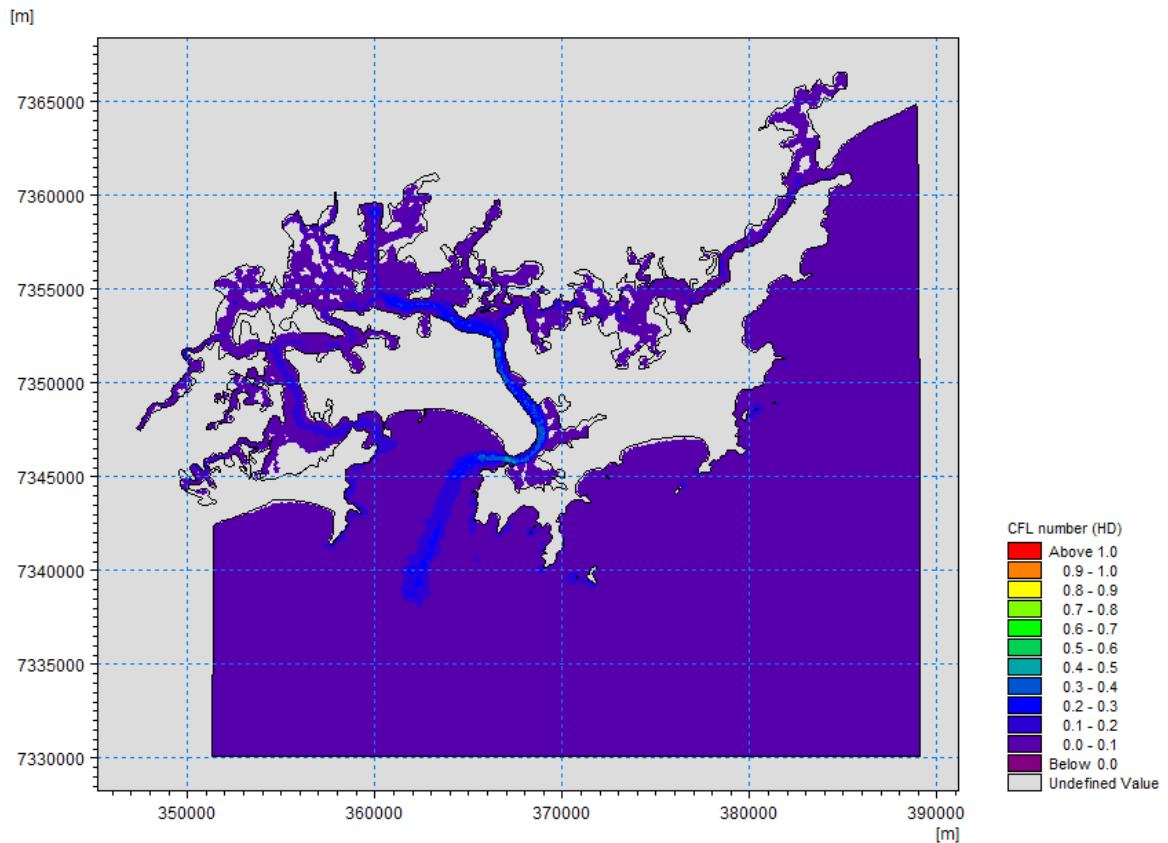


Figure 18 - Courant–Friedrichs–Lewy condition (CFL number) of Santos Estuary System and nearshore model.

The Figure 18 shows the CFL number in the entire domain of the model. Since, the condition $-1 \leq \text{CFL} \leq 1$ is checked, thus the model is stable.

Considering Lax Equivalence Theorem, the convergence is confirmed. Therefore, the model is ready to see the calibration and validation, and after to retrieve result from simulations.

7.3.4. Mesh Definition

The module Mike Mesh Generator, which constructs an unstructured mesh with triangular and quadrangular elements, performed mesh refinement. This module also divide the mesh into polygons with distinct properties such as maximum element size and type. Defining a triangular mesh with desirable result accuracy and acceptable model simulation time should avoid triangles with small angles (seeking equilateral triangles), smooth boundaries, and refine resolution in areas of interest.

The domain consists on several polygons that have elements with similar characteristics. The polygons were classified considering different areas, such as port channel, estuary channels, mangrove, bay and sea.

Areas of interest, where results will be retrieved from or where the simulated phenomenon requires mesh densification, have smaller polygons. Also, all mesh elements are

triangular and their angles are greater than 30° (degrees), whereas each polygon has a local maximum area element.

After model's results reached desirable accordance with field data for calibration, the final mesh (Table 8) and the final bed roughness were set (Figure 19). The 2006 model's unstructured mesh was set with 31,897 nodes and 57,039 elements. Figure 20 shows the domain discretization into triangular elements (unstructured mesh) and the variation of element density according to each polygon.

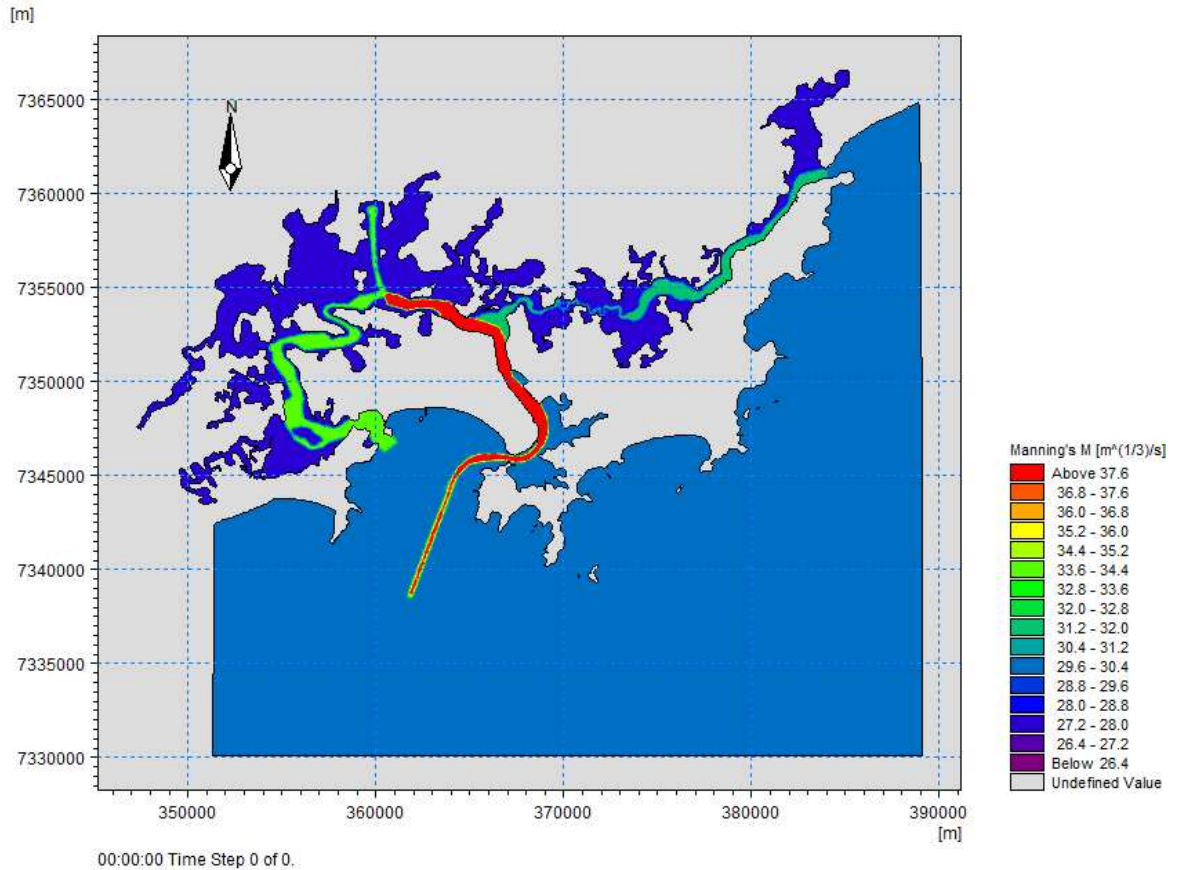


Figure 19 - Manning's M bed roughness map of Santos Estuary System and nearshore model.

Table 8 - Maximum element area (m^2) and Manning's M roughness ($m^{1/3}/s$) of Santos Estuary System hydrodynamic model according to the type of polygon.

Type of Polygon	Maximum Element Area (m^2)	Manning's M ($m^{1/3}/s$)	Manning's n ($s/m^{1/3}$)
Port Channel	2,500 – 6,000	34-38	0.026-0.029
Estuary Channels	5,000 – 7,500	32 – 34	0.029-0.031
Mangrove	10,000	28 – 30	0.033-0.036
Bay	50,000	30	0.033
Sea	200,000	30	0.033

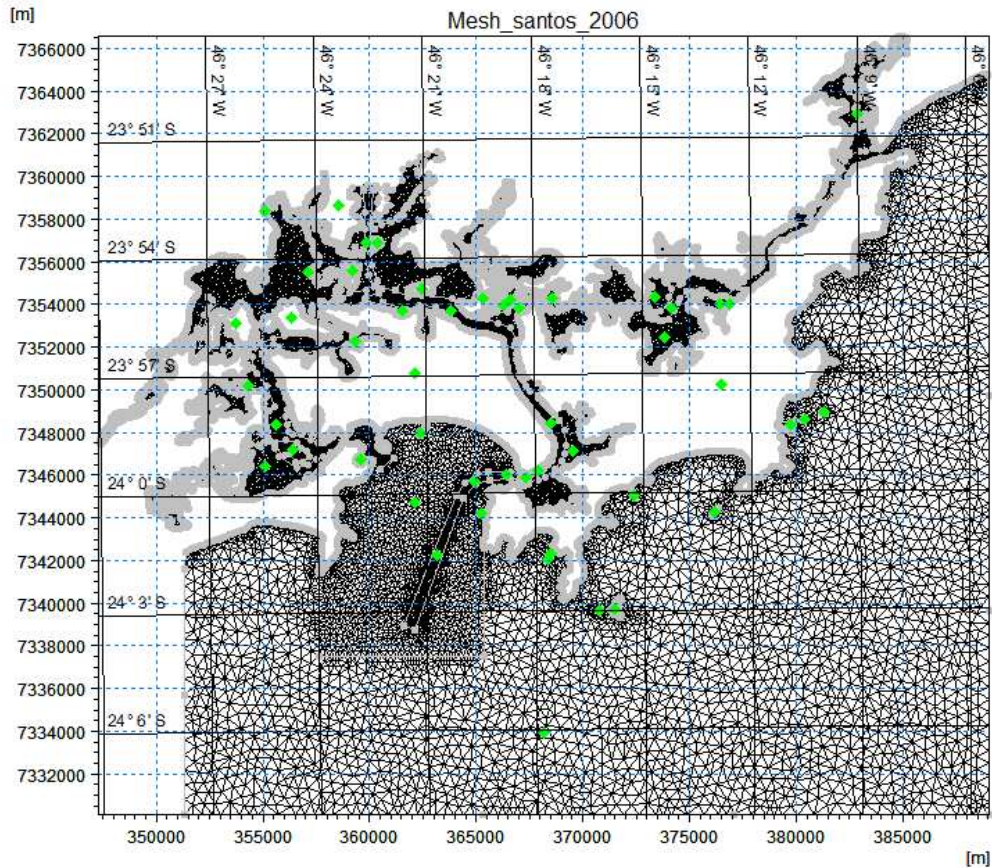


Figure 20 - Unstructured mesh of Santos Estuary System and nearshore model.

Table 9 shows that all the Manning's n values selected for each type of polygon (Table 8) is in accordance with Chow (1959) Manning's n for channels (Annex II.2).

Table 9 - Comparison between CHOW (1959) Manning's n roughness and Santos Estuary System hydrodynamic model Manning's n used for model calibration.

Hydrodynamic Model		CHOW (1959)			
Type of Polygon	Manning's n ($s/m^{1/3}$)	Type of channel	Manning's n		
			Minimum	Normal	Maximum
Port Channel	0.026-0.029	Dragline-excavated or dredged (no vegetation)	0.023	0.025	0.030
Estuary Channels	0.029-0.031	Main Channels (clean, straight, full stage, no rifts or deep pools)	0.025	0.030	0.033
Mangrove	0.033-0.036	Main Channels (clean, winding, some pools and shoals)	0.033	0.040	0.045
Bay	0.033	NA	NA	NA	NA
Sea	0.033	NA	NA	NA	NA

7.4. Model Calibration

The model calibration period of simulation covers 13 days, with 2 seconds of time step interval. The simulation start date is 1st May of 2004 (00h 00min) and the simulation end date is 14th May of 2004 (00h 00min). Therefore, the simulation has 561,600 time steps.

The calibration consisted on adjusting the bed roughness (Figure 19) to minimize the errors in each tide gauge station (Figure 21).

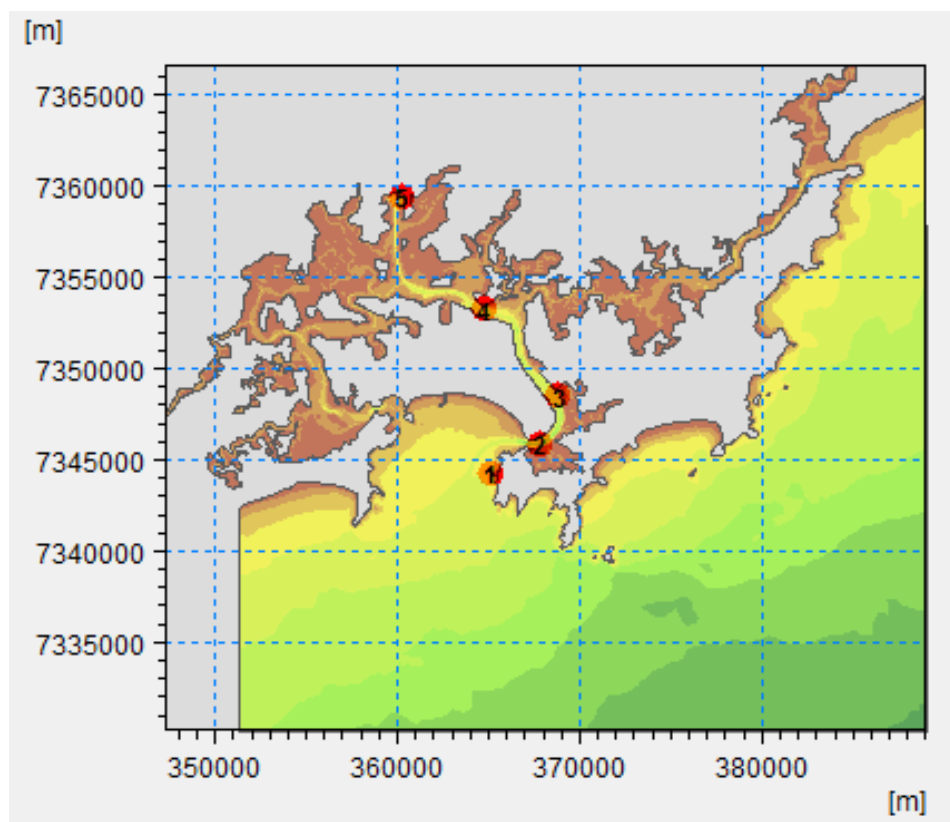


Figure 21 - Tide gauge stations along Santos estuary used to calibrate the hydrodynamic model. 1-Ilha das Palmas, 2-Praticagem, 3-Conceiçãozinha, 4-Ilha Barnabé and 5-Cosipa (Source: CORRÊA et al., 2018).

Each tide gauge has an observation time range (Table 10) and the raw data had been harmonically analyzed to retrieve the nine most energetic constituents (Q1, O1, P1, K1, N2, M2, S2, K2 and M3) in the five tide gauge stations (Table 11). The raw tide gauge data of stations (1), (3), (4) and (5) are from INPH (2007), and data from station (2) is from FEMAR (2000), the constituents were derived from Harmonical Analysis using PACMARE (FRANCO, 1988), referenced in the time zone UTC +0 (Coordinated Universal Time).

Table 10 - Period of tide gauge observation used in harmonical analysis of measured tidal elevation to retrieve amplitude and phase of the nine most energetic tide constituents (Q1, O1, P1, K1, N2, M2, S2, K2 and M3).

Tide Gauge	Initial observation date	Last observation date
(1) Ilha das Palmas	April 21 st , 2004	May 19 th , 2004
(2) Praticagem	September 5 th , 1995	October 7 th , 1995
(3) Conceiçãozinha	April 1 st , 2004	May 31 st , 2004
(4) Ilha Barnabé	April 9 th , 2004	May 15 th , 2004
(5) Cosipa	April 14 th , 2004	May 15 th , 2004

The results show good agreement with field data, the comparison between harmonic analysis and simulated results are shown in Figure 22 that correspond to (1) Ilha das Palmas, (2) Praticagem, (3) Conceiçãozinha, (4) Ilha Barnabé and (5) Cosipa, respectively.

Table 11 - Tide gauge stations used in the model calibration, and amplitude and phase for the constituents Q1, O1, P1, K1, N2, M2, S2, K2 and M3.

Constituent	A/Ph	Ilha das Palmas	Praticagem	Conceiçãozinha	Ilha Barnabé	Cosipa
Q1	(m)	0.0257	0.0480	0.0326	0.0320	0.0287
	(°)	83.82	83.00	80.81	85.87	100.94
O1	(m)	0.1104	0.1290	0.1119	0.1147	0.1193
	(°)	127.44	129.00	124.27	128.85	127.98
P1	(m)	0.0175	0.0220	0.0239	0.0220	0.0230
	(°)	169.27	193.00	174.74	167.72	162.86
K1	(m)	0.0529	0.0650	0.0723	0.0664	0.0696
	(°)	172.67	198.00	178.83	170.87	165.68
N2	(m)	0.0478	0.0470	0.0570	0.0493	0.0524
	(°)	223.58	232.00	216.97	222.02	237.38
M2	(m)	0.3379	0.3390	0.3766	0.3877	0.4030
	(°)	167.57	166.00	166.84	171.31	176.30
S2	(m)	0.2142	0.2490	0.2377	0.2484	0.2523
	(°)	169.10	176.00	171.83	174.62	179.67
K2	(m)	0.0583	0.0680	0.0647	0.0676	0.0686
	(°)	169.22	177.00	172.24	174.89	179.94
M3	(m)	0.0535	0.0520	0.0547	0.0613	0.0688
	(°)	347.04	343.00	339.93	351.89	3.60

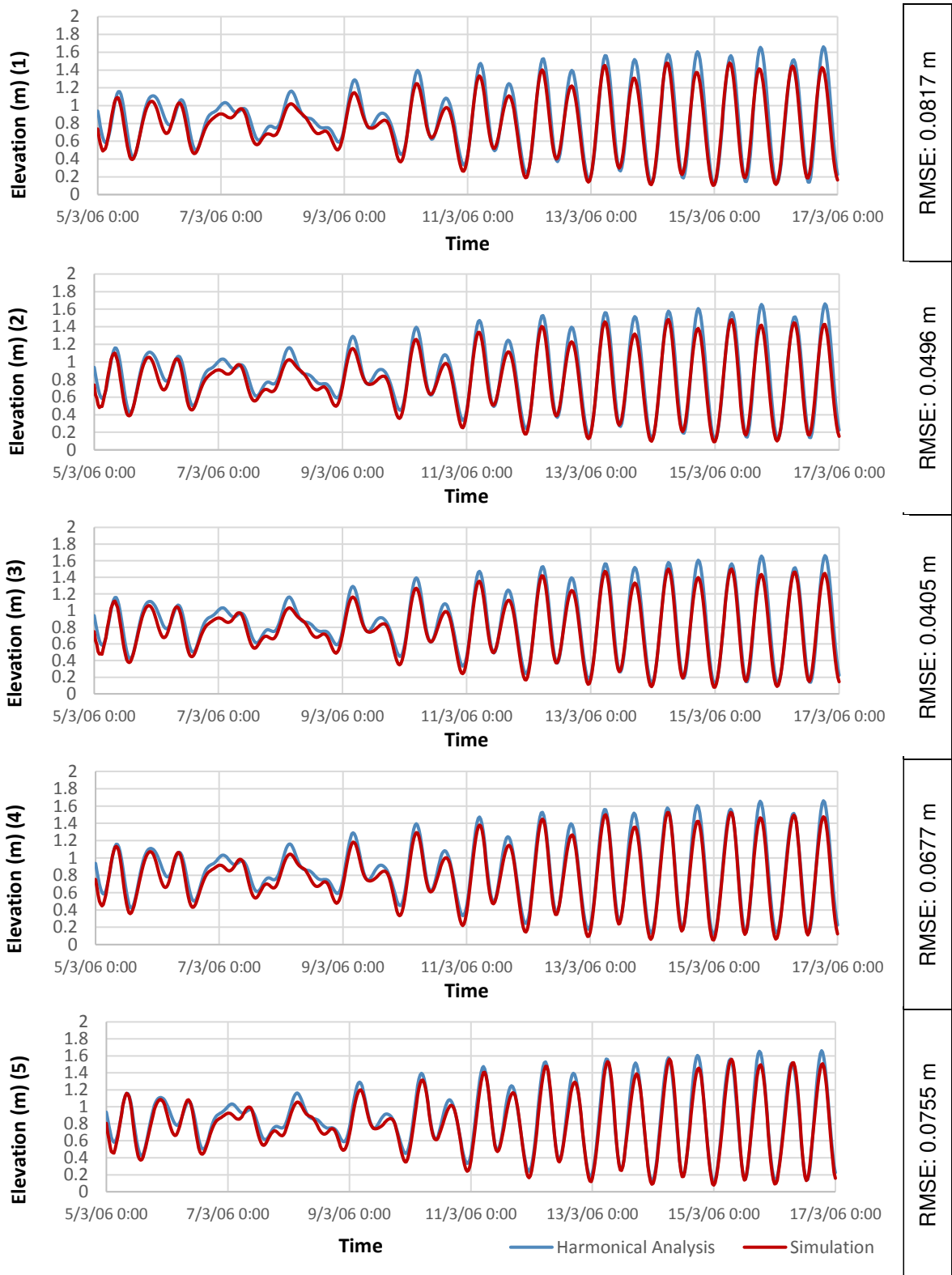


Figure 22 - Time series comparative between harmonic analysis (blue) and simulation (red) for tide gauge station (1) Ilha das Palmas, (2) Praticagem, (3) Conceiçãozinha, (4) Ilha Barnabé e (5) Cosipa (Source: CORRÊA et al., 2018).

The time series error evaluation must be consistent with the data pattern. Since tides have sinusoidal behavior, mean error can be dismissive. Thus, the Root Mean Square Error (RMSE) is the most suitable error measure to evaluate this data. Moreover, RMSE (Equation 17) is widely used in physical sciences such as Oceanography and Meteorology.

$$RMSE = \sqrt{\frac{\sum_{t=1}^n (S_t - O_t)^2}{n}} \quad \text{Equation 17}$$

Where: t is the time step, n is the amount of data acquired or the sample size, S are the simulated values, and O are the observed values. RMSE is easy to understand because it has the same metric as S and O (Willmott, 1981).

According to WILLMOTT (1981) the Index of Agreement, also known as SKILL, (Equation 18) is not a dimensionless measure of correlation. In fact, it reflects the degree to which the observed variate is accurately simulated, and it varies from 0 (no agreement) to 1 (total agreement) (WILLMOTT, 1981; HARARI, 2015). Figure 23, Figure 24, Figure 25, Figure 26 and Figure 27 show the agreement between harmonical analysis and simulation.

$$SKILL = 1 - \frac{\sum_{t=1}^n (S_t - O_t)^2}{\sum_{t=1}^n (|S_t - \bar{S}| + |O_t - \bar{O}|)^2} \quad \text{Equation 18}$$

Where: t is the time step, n is the amount of data acquired or the sample size, S are simulated values, \bar{S} are the average of simulated values, O are observed values and \bar{O} is the average of observed values (Willmott, 1981).

Both, RMSE and SKILL (Index of Agreement) confirm the reliability of this hydrodynamic model, since it was capable of reproducing tidal elevations along Santos estuary. It is noticeable that higher tidal elevation values present higher deviation, which means higher error. Though, the Agreement Index and RMSE still acceptable for the study purpose.

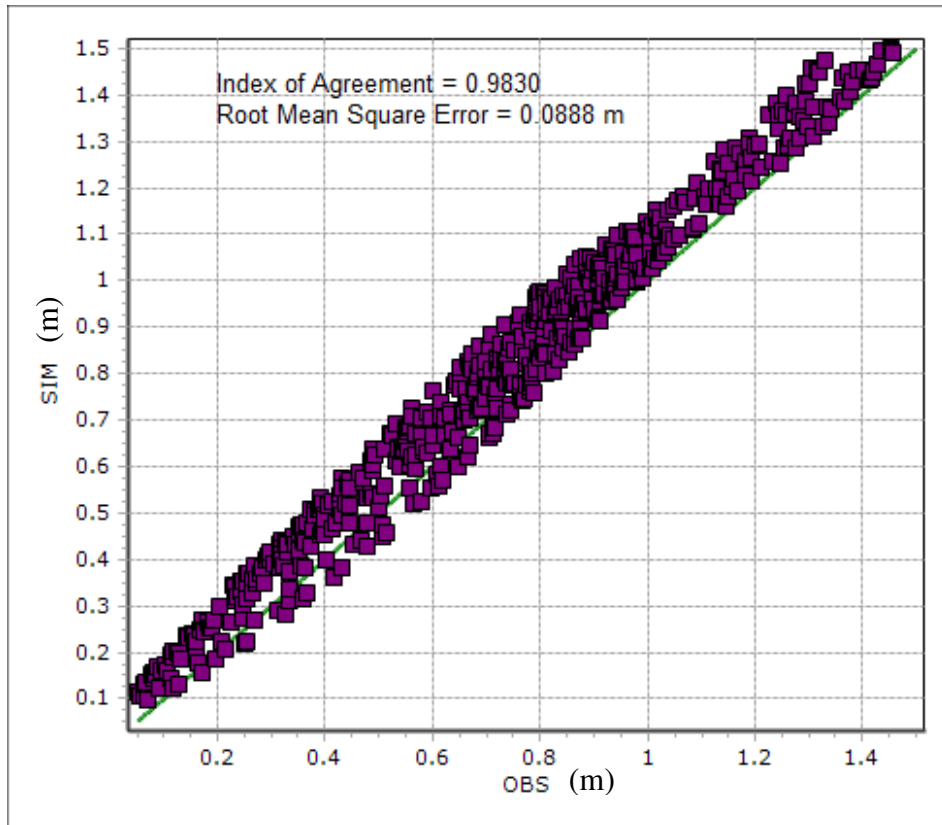


Figure 23 - Time series error between harmonical analysis (OBS) and simulation (SIM) for tide gauge station (1) Ilha das Palmas (RMSE = 0.0888 m and Agreement Index = 0.9830).

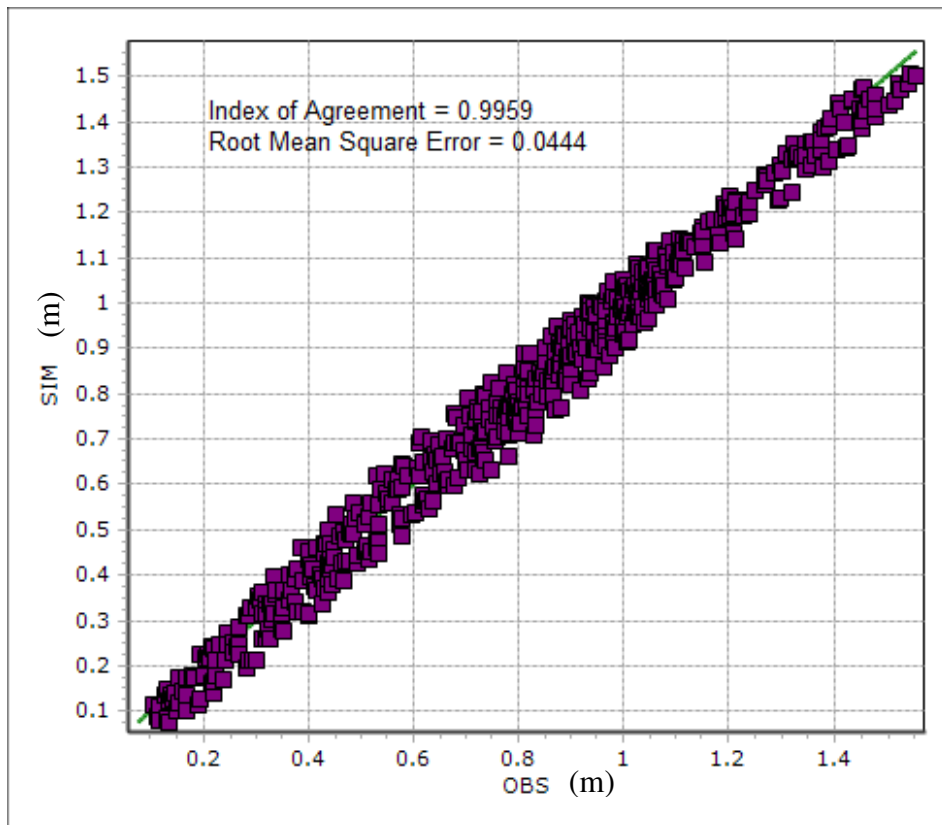


Figure 24 - Time series error between harmonical analysis (OBS) and simulation (SIM) for tide gauge station (2) Praticagem (RMSE = 0.0444 m and Agreement Index = 0.9959).

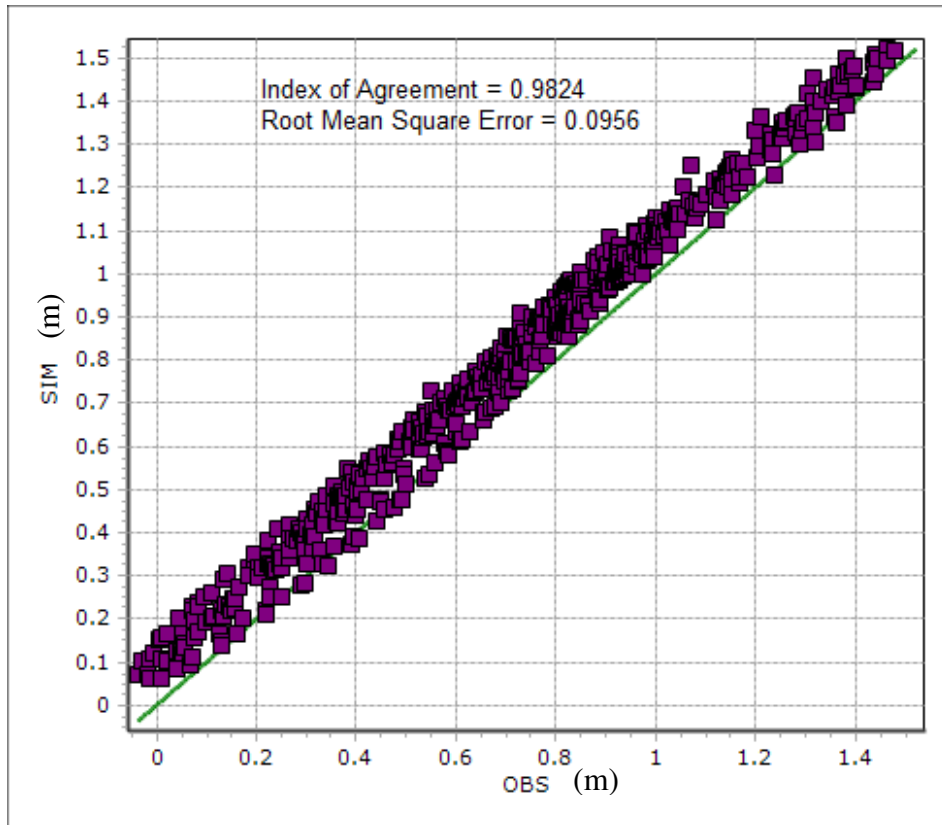


Figure 25 - Time series error between harmonical analysis (OBS) and simulation (SIM) for tide gauge station (3) Conceiçãozinha (RMSE = 0.0956 m and Agreement Index = 0.9824).

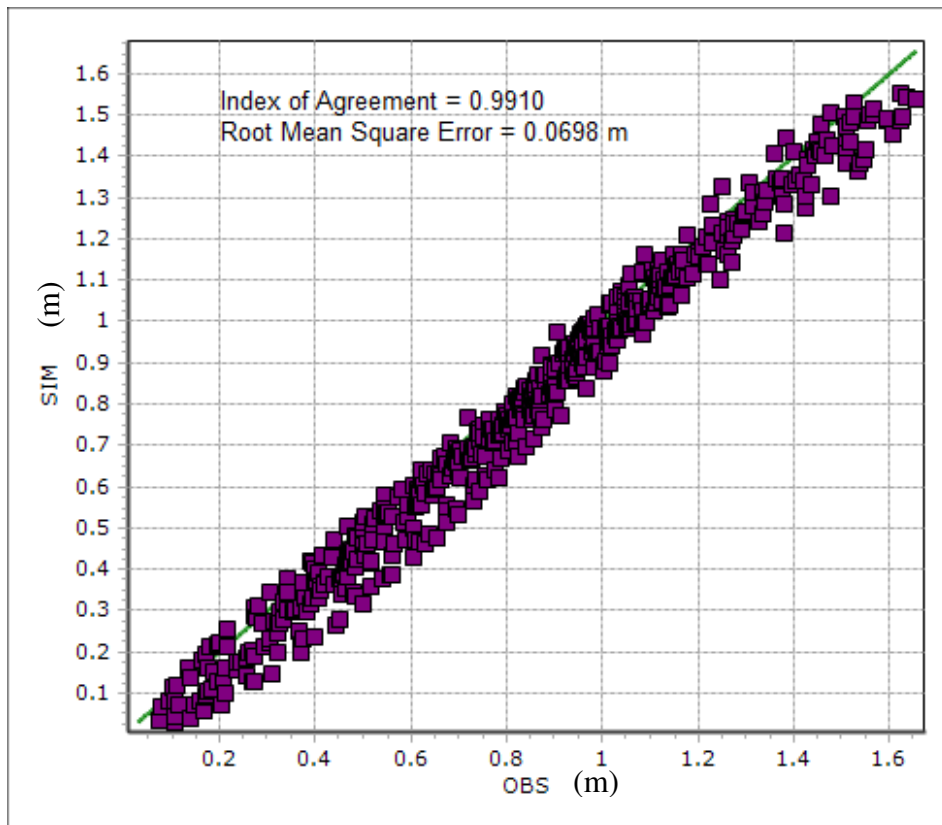


Figure 26 - Time series error between harmonical analysis (OBS) and simulation (SIM) for tide gauge station (4) Ilha Barnabé (RMSE = 0.0698 m and Agreement Index = 0.9910).

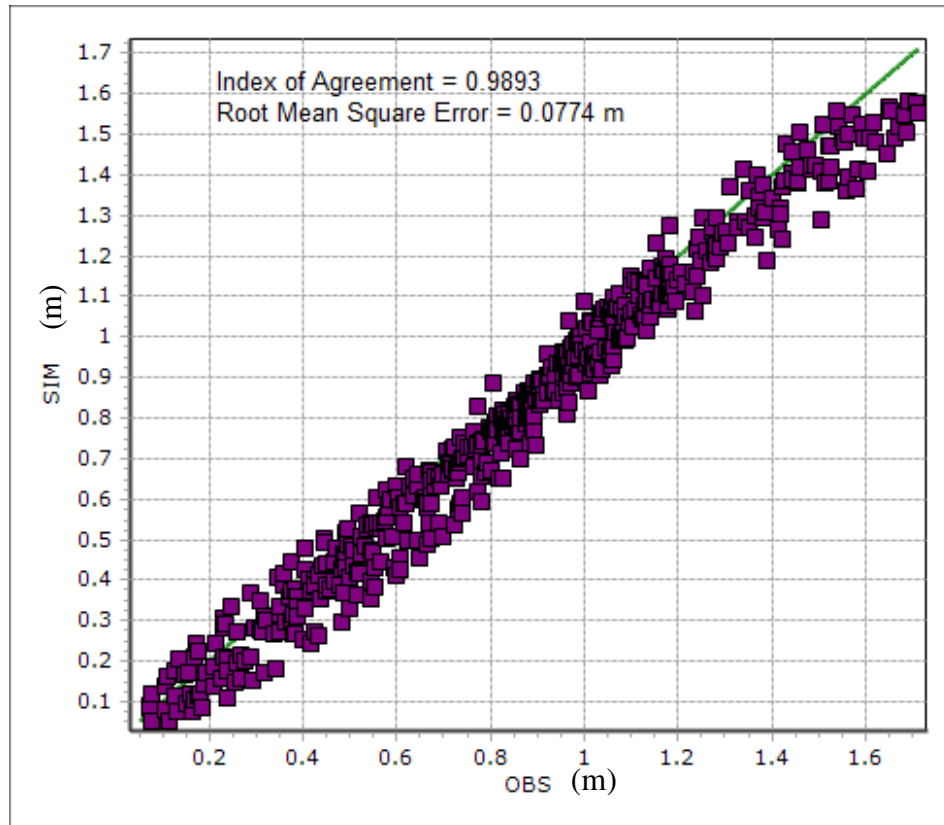


Figure 27 - Time series error between harmonical analysis (OBS) and simulation (SIM) for tide gauge station (5) Cosipa (RMSE = 0.0774 m and Agreement Index = 0.9893).

The comparison of the nine tidal constituents (Q1, O1, P1, K1, N2, M2, S2, K2 and M3), derived from harmonical analysis of FEMAR (2000) tide gauges records and of time series generated by the hydrodynamic model, show reasonable agreement between amplitude and phase for Ilha das Palmas (Table 12), Praticagem (Table 13), Conceiçãozinha (Table 14), Ilha Barnabé (Table 15) and Cosipa (Table 16).

Table 12 - Comparison between amplitude (cm) and phase (°) of nine constituents as given by Ilha das Palmas tide gauge records (FEMAR, 2000) and time series generated by hydrodynamic model.

Tidal constituent	(1) Ilha das Palmas		Simulation	
	Ampl. (cm)	Phase (°)	Ampl. (cm)	Phase (°)
Q1	3.20	73.00	4.00	93.70
O1	9.60	126.00	11.94	121.18
P1	2.20	149.00	2.95	183.16
K1	6.70	151.00	8.90	188.19
N2	4.60	234.00	2.34	214.32
M2	35.30	168.00	34.65	177.52
S2	22.90	165.00	25.12	182.69
K2	6.20	165.00	6.83	183.10
M3	4.50	328.00	5.19	337.35

Table 13 - Comparison between amplitude (cm) and phase (°) of nine constituents as given by Praticagem tide gauge records (FEMAR, 2000) and time series generated by hydrodynamic model.

Tidal constituent	(2) Praticagem		Simulation	
	Ampl. (cm)	Phase (°)	Ampl. (cm)	Phase (°)
Q1	4.80	83.00	3.94	94.89
O1	12.90	129.00	12.16	122.43
P1	2.20	193.00	3.00	184.96
K1	6.50	198.00	9.07	190.03
N2	4.70	232.00	2.27	212.35
M2	33.90	166.00	35.29	180.48
S2	24.90	176.00	25.72	185.48
K2	6.80	177.00	7.00	185.88
M3	5.20	343.00	5.48	343.63

Table 14 - Comparison between amplitude (cm) and phase (°) of nine constituents as given by Conceiçãozinha tide gauge records (FEMAR, 2000) and time series generated by hydrodynamic model.

Tidal constituent	(3) Conceiçãozinha		Simulation	
	Ampl. (cm)	Phase (°)	Ampl. (cm)	Phase (°)
Q1	3.26	80.81	3.90	97.06
O1	11.19	124.27	12.30	122.50
P1	2.39	174.74	3.02	185.88
K1	7.23	178.83	9.13	191.02
N2	5.70	216.97	2.08	214.54
M2	37.66	166.84	36.18	183.10
S2	23.77	171.83	26.44	188.01
K2	6.47	172.24	7.19	188.41
M3	5.47	339.93	5.77	348.93

Table 15 - Comparison between amplitude (cm) and phase (°) of nine constituents as given by Ilha Barnabé tide gauge records (FEMAR, 2000) and time series generated by hydrodynamic model.

Tidal constituent	(4) Ilha Barnabé		Simulation	
	Ampl. (cm)	Phase (°)	Ampl. (cm)	Phase (°)
Q1	2.50	91.00	3.92	98.39
O1	11.40	125.00	12.45	123.44
P1	2.10	197.00	3.09	186.90
K1	6.20	205.00	9.33	192.05
N2	5.10	231.00	1.89	226.76
M2	38.40	173.00	38.13	186.66
S2	23.30	178.00	27.60	191.51
K2	6.30	178.00	7.51	191.90
M3	5.50	15.00	6.26	356.03

Table 16 - Comparison between amplitude (cm) and phase (°) of nine constituents as given by Cosipa tide gauge records (FEMAR, 2000) and time series generated by hydrodynamic model.

Tidal constituent	(5) Cosipa		Simulation	
	Ampl. (cm)	Phase (°)	Ampl. (cm)	Phase (°)
Q1	3.70	95.00	3.90	97.06
O1	13.10	130.00	12.30	122.50
P1	1.90	208.00	3.02	185.88
K1	5.70	208.00	9.13	191.02
N2	6.50	244.00	2.08	214.54
M2	37.70	178.00	36.18	183.10
S2	23.70	184.00	26.44	188.01
K2	6.40	184.00	7.19	188.41
M3	6.80	20.00	5.77	348.93

7.5. Model Validation

The model validation period of simulation covers 13 days, with 2 seconds of time step interval. The simulation start date is 4th March of 2006 (00h 00min) and the simulation end date is 17th March of 2006 (00h 00min). Therefore, the simulation has 561,600 time steps.

Due to lack of data availability, the period of validation covers 8 days, from 9th to 17th March of 2006, so the first five days were simulated to guarantee the model equilibrium.

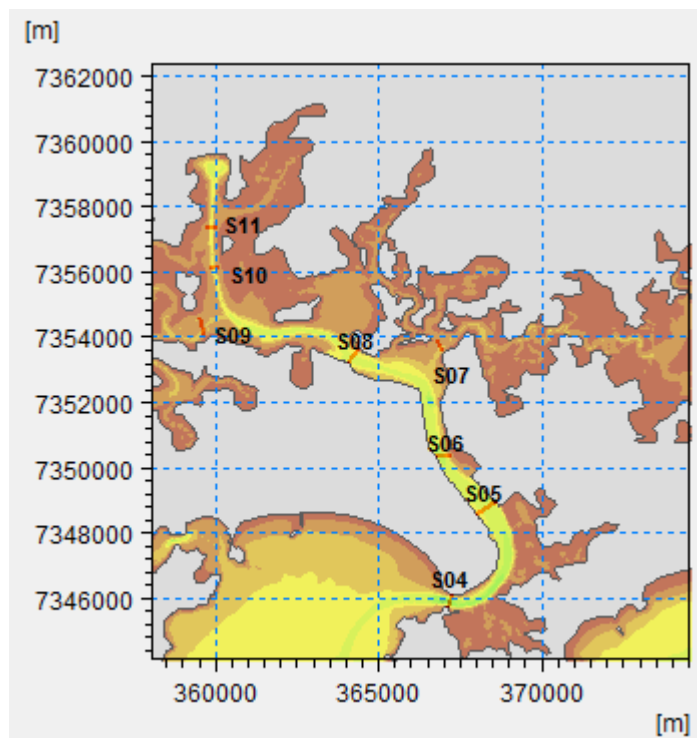


Figure 28 - Eight flow measurement sections (S04, S05, S06, S07, S08, S09, S10, S11) along Santos estuary used to validate the hydrodynamic model for currents.

INPH (2007) measured the current velocities *in situ* along Santos estuary using ADCP (Acoustic Doppler Current Profile). The validation consisted of comparing the mean flow

velocity in eight sections (INPH, 2007) along the estuary (Figure 28) with current velocities retrieved from model simulation. The validation consists only on comparing results, no adjustments are allowed during this process.

The validation results show good or acceptable agreement with measured values from flow stations along Santos Estuary (Figure 29). The error evaluation was based on Index of Agreement (Equation 18), also known as SKILL, which is widely used to assess flow validity in hydrodynamic numerical modelling (COELHO, 2009; WARNER *et al.*, 2005; HARARI, 2015).

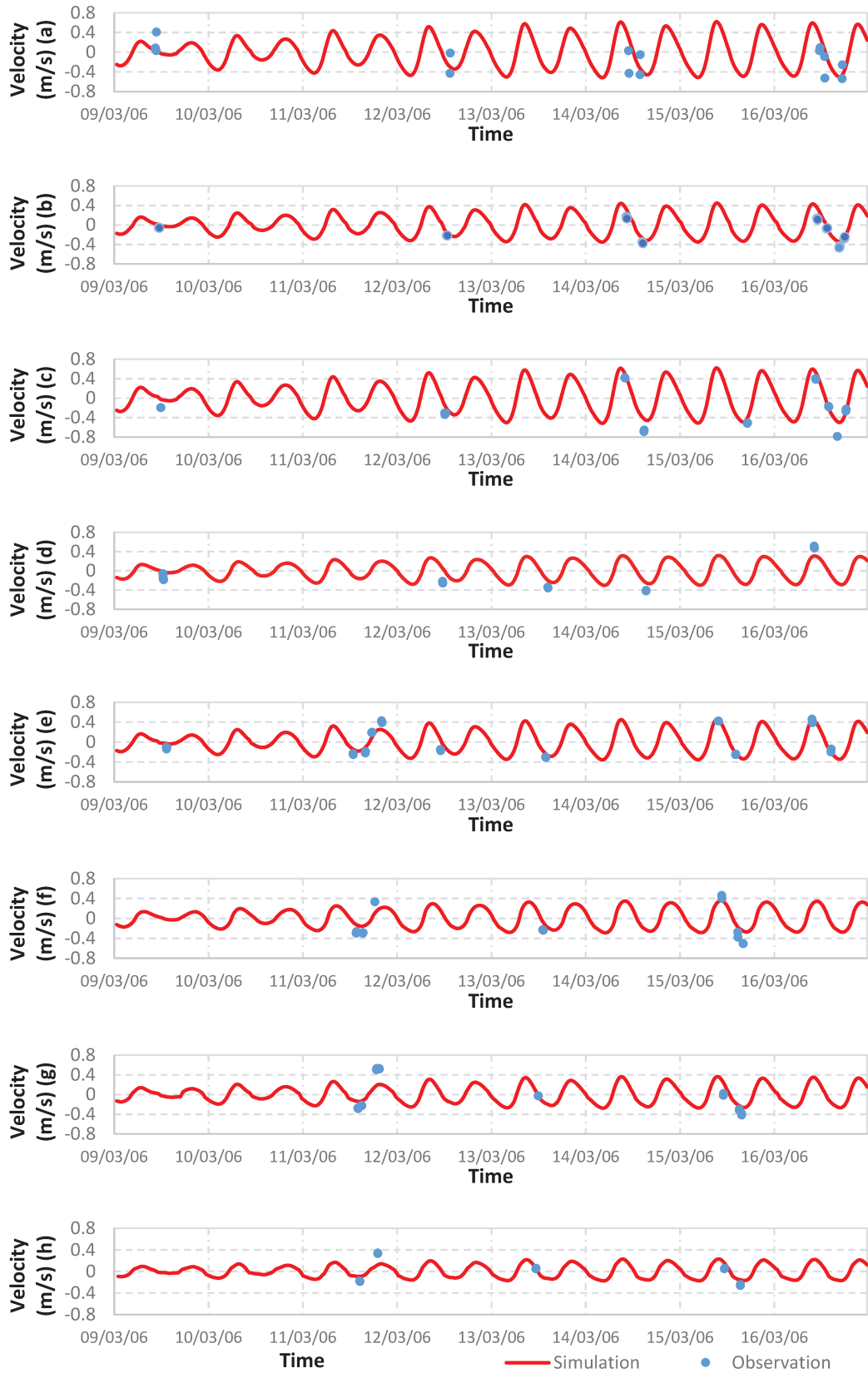


Figure 29 - Model validation for flow measurement sections S04 (a), S05 (b), S06 (c), S07 (d), S08 (e), S09 (f), S10 (g), S11 (h). Comparative between flow measurement (blue) and simulation (red).

All flow stations were expected to present errors because the model considers only nine tidal constituents, and the flow measurements are influenced by meteorological tide and salinity as well (INPH, 2007). Moreover, the flow measurement is not continuous, so it is not possible to determine the tidal current velocity behavior based on the available data.

Despite no reference set a threshold for Skill score for flow velocity validity, scores above 0.65 are considered good and values above 0.45 are acceptable (COELHO, 2009). Figure 30 shows that flow stations S04, S05, S06, S07, S08 and S09 SKILL are higher than 0.8, and flow stations S10 and S11 are higher than 0.6.

Skill score for S07 and S09 flow stations may be lower because the bathymetry has coarser scatter data in this area. Moreover, São Vicente Estuary and Bertioga Estuary hydraulics affect S07 and S09 flow measurements, respectively.

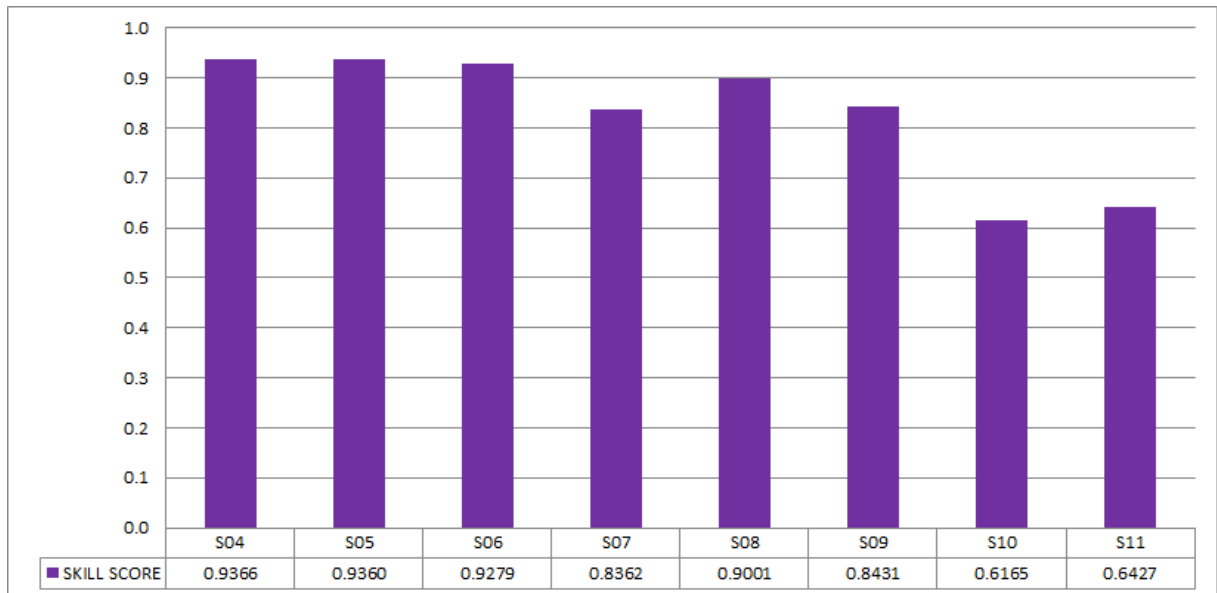


Figure 30 - Skill score for each flow station along Santos Estuary: S04=0.9366; S05=0.9360; S06=0.9279; S07=0.8362; S08=0.9001; S09=0.8431; S10=0.6165; S11=0.6427.

8. STABILITY OF SANTOS ESTUARY INLET

As discussed in sections 5.1.2 and 5.1.3, deepening dredging tends to increase tidal prism, while land reclamation tends to decrease tidal prism. Therefore, four scenarios were simulated using hydrodynamic modelling.

The baseline scenario has no additional port terminals, thus no additional land reclamation, and the bathymetry applied to Port of Santos navigation channel surveyed in 2006 (Figure 8), before the deepening dredging. The other three scenarios are combinations of changes within Santos Estuary between 2006 and 2014: the Phase 1 of Port of Santos navigation channel deepening dredging (see Table 2), and the construction of two port terminals (see section 3.2.2). Since the objective of this study is evaluating the effects of deepening dredging and land reclamation on Santos Estuary inlet, the tidal forcing are the same for all scenarios. Table 17 shows a brief description of each scenario, the scenarios before deepening dredging have bathymetry from 2006, while the scenarios after deepening dredging have bathymetry from 2014.

Table 17 - Brief description of scenarios simulated with hydrodynamic model.

Scenario	Bathymetry	Land reclamation
A (Baseline 2006)	Before deepening dredging	No reclamation
B (only land reclamation)	Before deepening dredging	Additional port terminals
C (only deepening dredging)	After deepening dredging	No reclamation
D (combined)	After deepening dredging	Additional port terminals

8.1. Calibration of Area-Prism relationship coefficients using Slice Method

Following the Slice Method described in section 6, Santos estuary inlet was divided into 43 slices, and the specific discharge time series of each slice was retrieved from the hydrodynamic numerical model described in section 7. Then, tidal prism was computed during each tidal period (consecutive flood and ebb water slacks). For scenario A (Baseline), the larger Spring Tidal Prism for the simulated period summed a volume of 55.1×10^6 m.

As a reference, SONDOTECNICA (1977a) computed the tidal prism for Santos Estuary inlet using a geometrical method. They defined the tidal truncation in São Vicente estuary and in Bertioaga estuary, then measured the surface area of the estuary and multiplied by the tidal range in the entrance of the estuary. According to field surveys conducted by SONDOTECNICA (1977a) in August 25th of 1976, the estuary surface area was 36.1×10^6 m² and the tidal range at the entrance of the estuary was 1.52 m. Thus, the tidal prism in that occasion was 54.9×10^6 m³. Therefore, the tidal prism computed for Scenario A has the same order of magnitude of this estimate.

During the tidal period related to the Spring Tidal Prism of Scenario A, the slice tidal prism (ΔP) was computed using Equation 7 for the 43 slices (each with $\Delta L = 7.7$ m) of Santos estuary inlet cross-sectional area, and then plotted with their corresponding slices areas (ΔA computed using Equation 10) (Figure 31).

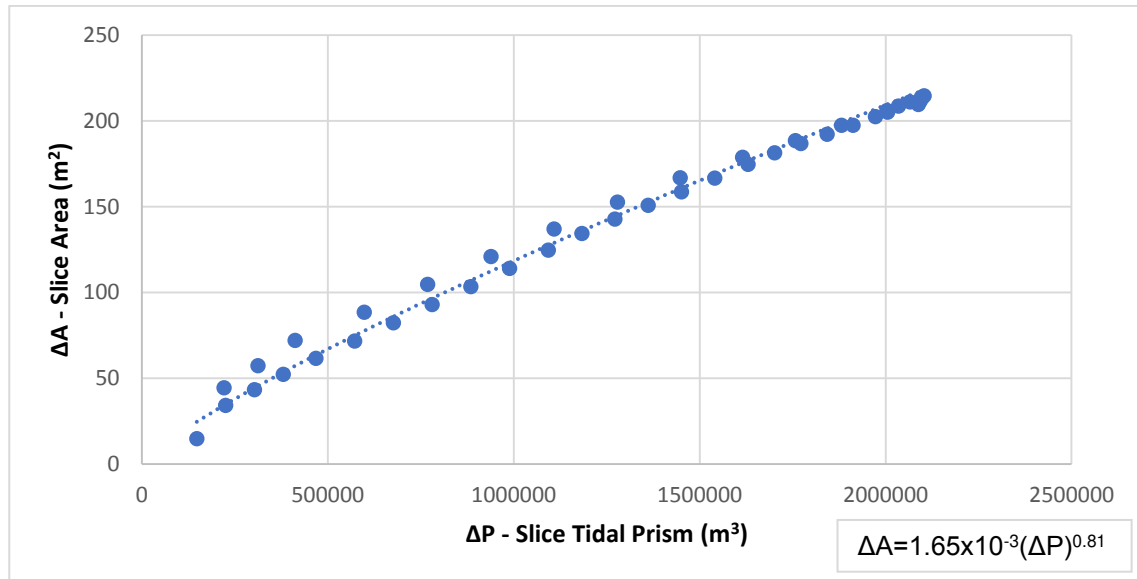


Figure 31 - AP relationship for Santos estuary tidal inlet derived from the Slice Method, and potential trend line for scatter data.

The calibration of coefficients C and q followed the steps described in the section 6.2, by using a non-linear optimization model to minimize the sum of the square of the differences between measured (ΔA_i) and computed ($\overline{\Delta A}_i$) area for each slice (Equation 9). Thus, the coefficients that best fit the scatter data are $C=1.65 \times 10^{-3}$ and $q=0.81$ (Figure 31). These coefficients seem reasonable, considering HUME AND HERDENDORF (1993) comprehensive investigation on 80 New Zealand inlets, the category which presents the most similar coefficients to Santos coefficients is “River mouth” (see Table 4).

8.2. Validation of Area-Prism relationship using Slice Method

The cross-sectional area of Scenario A (baseline from 2006) and of Scenario D (with two additional port terminals and deepening dredging from 2014) must be validated before using the coefficients of Santos estuary inlet Area-Prism relationship ($C=1.65 \times 10^{-3}$ and $q=0.81$) for other scenarios.

The cross-sectional area for Scenario A (baseline 2006) and for Scenario D (combined) are estimated by the sum of the 43 slices using the Area-Prism relationship defined by the Slice Method (Equation 11). The geometry of each slice is approximated to a trapezium, two consecutive depths are the bases (trapezium with parallel sides) and the slice width (Δl) is the orthogonal edge of the parallel bases.

Table 18 – Estimates of Santos estuary tidal inlet cross-sectional area for Scenario A (baseline 2006) and Scenario D (2014).

Scenario (Year)	Cross-sectional Area (m ²)		Relative error (%)	Tidal Prism (m ³)
	Field data	Slice Method		
A (Baseline 2006)	6,105	6,132	+0.4	55.1x10 ⁶
D (combined)	5,769	6,021	+4.4	53.6x10 ⁶
Area reduction	5.5%	1.8%	-	-

Santos estuary tidal prism reduced by 2.7% from $55.1 \times 10^6 \text{ m}^3$ to $53.6 \times 10^6 \text{ m}^3$. The reduction of Santos estuary inlet cross-sectional area due to combined effect of land reclamation and deepening dredging is confirmed by field data and by Slice Method: both approaches show that Santos estuary tidal inlet cross-sectional area reduced from 2006 to 2014 (Table 18). This result is consistent with other cases, where cumulative land reclamation reduced tidal prism (CUVILLIEZ et al., 2009; FENG et al., 2015).

Despite deepening dredging tends to increase tidal prism (OLIVEIRA et al, 2009; MALHADAS et al, 2009; PICADO et al. 2010), Santos estuary tidal prism reduced between 2006 and 2014. Therefore, in this case, land reclamation effect on tidal prism reduction overlapped deepening dredging opposite effect.

Regarding tidal inlet cross-sectional area, the Slice Method estimated a lesser reduction (1.8%) compared to the actual reduction (5.5%) from 2006 to 2014 (Table 18 and Figure 32, also Appendix 1.1 shows the computation of cross-sectional area of all 43 slices).

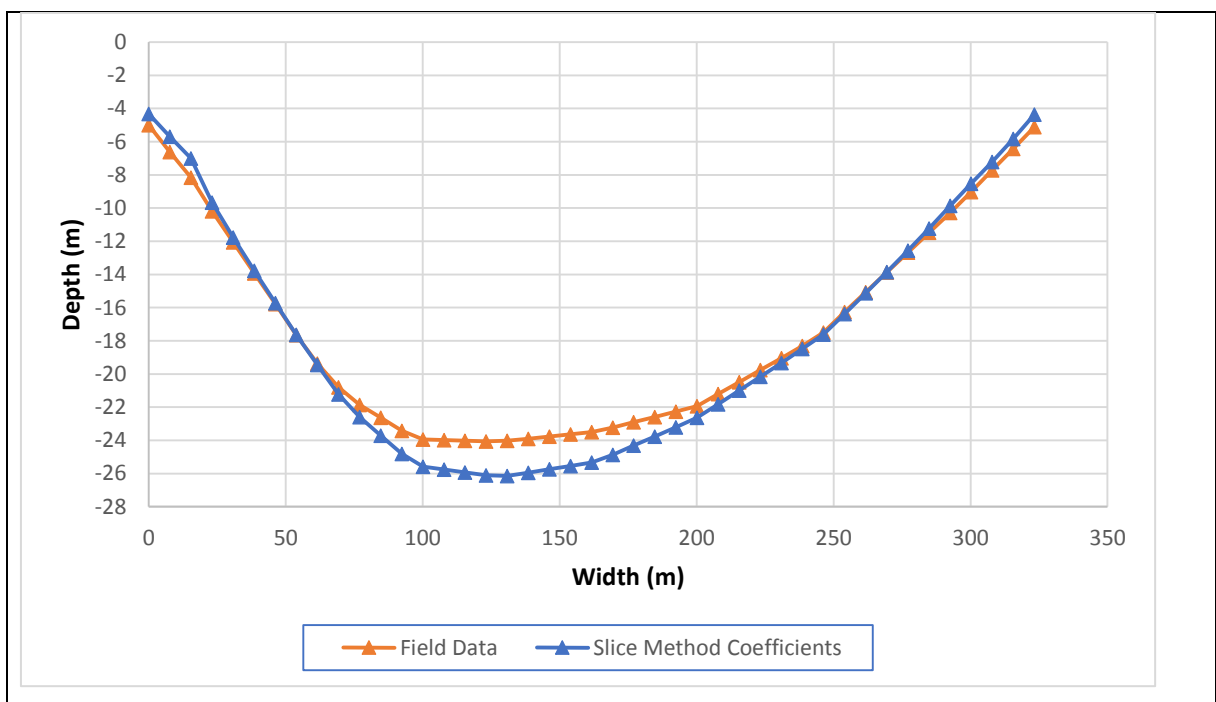


Figure 32 - Comparison between real and estimated cross-sectional profiles in 2014.

Only land reclamation and deepening dredging in Santos estuary were accounted as changes in bathymetry, so changes and responses from mangrove and interventions in São Vicente and Bertioga estuarine channels were not updated. These areas also affect Santos estuary tidal prism. Thus, outdated areas might explain why the Slice Method cross-sectional area reduction estimative is lower than actual reduction.

Moreover, tidal inlet may take decades to adapt from land reclamation and reach its stability (VAN DE KREEKE, 2004; OOST, 1995). Despite Santos estuary tidal inlet may be

under adaptation, field data and the Slice Method confirm that tidal inlet got shallower and during this short period of eight years.

8.3. The isolated effects of land reclamation and deepening dredging

The Spring Tidal Prisms estimated for Scenarios A, B, C and D followed the steps of Step Method described in section 6.1, and finally the partial tidal prism of 43 slices were summed using Equation 8. The Appendix 1.1 shows the partial tidal prism of all 43 slices and the sum of them, the tidal prism, and Table 19 shows the tidal prism for each scenario.

Table 19 - Tidal Prism and cross-sectional area estimates for all proposed scenarios using Slice Method.

Scenario	Tidal Prism (m ³)	Area (m ²)
A (Baseline 2006)	55.1x10 ⁶	6,132
B (only reclamation)	53.4x10 ⁶	5,997
C (only deepening dredging)	55.3x10 ⁶	6,175
D (combined)	53.6x10 ⁶	6,021

As expected in section 5.1.3, the isolate effect of land reclamation (Scenario B) is the decrease of tidal prism, and the expected stable cross-sectional area is smaller than baseline's cross-sectional area. This result is in accordance with other case studies that observed reduction in tidal prism due to construction of port terminals and harbor facilities in estuaries, bays and lagoons (FENG *et al.*, 2015; CUVILLIEZ *et al.*, 2009; WAL *et al.*, 2002; LIRIA *et al.*, 2009; SHI *et al.*, 2011).

On the other hand, the isolated effect of deepening dredging (Scenario C) is the increment of tidal prism, as expect in section 5.1.2. This result is in accordance with other case studies which observed that deepening dredging increases tidal prism, and then leads to an enlargement of the cross-sectional area (CLEARY; FITZGERALD, 2003; MALHADAS *et al.*, 2009).

8.4. Testing different Area-Prism relationship coefficients for Slice Method

Slice Method consists of applying Area-Prism relationship for slices of the inlet cross-section, and then summing all of them to estimate the entire cross-section area. Herein two approaches are compared: (i) the classical, which applies Area-Prism relationship for the entire inlet cross-section, and (ii) Slice Method, which applies Area-Prism relationship for several slices of the same inlet and then sums all slices to estimate the entire inlet cross-sectional area.

Thus, two empirical coefficients and one theoretical coefficient were tested to estimate Santos estuary inlet cross-sectional area. The empirical coefficients adopted were (i) JARRETT (1976) for all inlets in the US (coefficients reprocessed by STIVE *et al.* (2010) to convert C and q for International System), and (ii) HUME AND HERDENDORF (1993) for River

Mouth in New Zealand. Also, HUGHES (2002) theoretical coefficients are tested. Using Equation 3, the coefficient C was calculated using data from Santos estuary, where $T=43,200$ s (tidal period), $d_e=0.11$ mm (median grain size), $W=385$ m (inlet width), $g=9.81$ m/s² (gravity acceleration), $S=2.65$ (sediment specific gravity), and $k_a=1$ (coefficient related to the effects of non-sinusoidal tide).

First, the classical Area-Prism relationship (Equation 2) is used to estimate the entire cross-sectional area (A) in function of tidal prism ($P=55.1 \times 10^6$). Table 20 shows the estimates of Santos estuary inlet cross-sectional area applying Area-Prism relationship for the entire cross-section and the relative error when compared to the cross-sectional area of 6,105 m² from bathymetric survey from 2006.

Table 20 - Estimative of Santos estuary tidal inlet cross-sectional area using the Area-Prism relationship with JARRETT (1976), HUGHES (2002) and HUME AND HERDENDORF (1993) coefficients.

Coefficient	C	q	Cross-sectional Area (m ²)	Relative error (%)
JARRETT (1976)	2.41×10^{-4}	0.93	3,813	-37.6
HUGHES (2002)	5.78×10^{-4}	0.89	4,482	-26.6
HUME AND HERDENDORF (1993)	4.39×10^{-3}	0.757	3,180	-47.9

Then, Equation 10 was applied to provide the area of each slice (ΔA_i), and then these slices were summed to estimate the total cross-sectional area (A) (Equation 11), Appendix 1.2 shows the partial tidal prism of all 43 slices and how each slice (ΔA_i) was calculated using the chosen Area-Prism relationship coefficients. Table 21 shows the estimate of Santos estuary inlet cross-sectional area using Slice Method and the relative error when compared to the cross-sectional area of 6,105 m² from bathymetric survey from 2006.

Table 21 - Estimative of Santos estuary tidal inlet cross-sectional area using the Slice Method with different coefficients.

Coefficient	C	q	Cross-sectional Area (m ²)	Relative error (%)
JARRETT (1976)	2.41×10^{-4}	0.93	4,912	-19.5
HUGHES (2002)	5.78×10^{-4}	0.89	6,678	+9.4
HUME AND HERDENDORF (1993)	4.39×10^{-3}	0.757	7,703	+26.6

Comparing results from Table 20 and Table 21, all Area-Prism coefficients had better estimates when applied to slices (ΔA_i) of the cross-sectional area. Also, HUGHES (2002) coefficients had better accuracy when compared to the other coefficients. This may occur because this approach uses local data to define the coefficient C , such as tidal period, median grain size, inlet width and sediment specific gravity, while the empirical approach consists of deriving the coefficients C and q from observation of several inlets.

9. CONCLUSION

By dividing the inlet into several slices, the Slice Method enhanced the estimative of tidal inlet cross-sectional area. Also, the calibration of coefficients C and q were improved by minimizing the sum of the square of the differences between measured (ΔA_j) and computed ($\overline{\Delta A_j}$) slice areas.

Therefore, the Slice Method provided a reasonable estimative of cross-sectional profile, making possible the evaluation of tidal inlet geometry changes. Even using JARRETT (1976), HUME AND HERDENDORF (1993) AND HUGHES (2002) coefficients, the results were more accurate than the application of Area-Prism relationship to the entire tidal inlet.

Santos estuary tidal prism reduced from 55.1×10^6 in 2006 to 53.6×10^6 in 2014, and the cross-sectional area reduced 5.5%. These observations support the assumption that the inlet stability decreased due to land reclamation, even with the deepening dredging combined. The estimate of cross-sectional area reduction using Slice Method could be more accurate if the bathymetry of mangrove, and São Vicente and Bertioga estuarine channels were updated. Nevertheless, the Slice Method estimated Santos estuary inlet area with reasonable accuracy, only 4.4% larger than the real area in 2014. Moreover, the cross-sectional profile estimate is consistent with field data investigations; both identified that tidal inlet got shallower.

Since land reclamation affects tidal prism, slight changes in estuarine lands may bring major effects in tidal inlet stability. Then, future Environment Impact Assessment of estuarine occupations in Santos estuary must consider the cumulative effects of land reclamation on tidal inlet stability in order to mitigate channel siltation and possible impacts on adjacent shoreline.

10. REFERENCES

- ACP. Expansion program. In: *Panama Canal Authority*. [S.l.]: Autoridad del Canal de Panamá, 2016.
- ACP. *First-Ever LNG Vessel Transits the Expanded Panama Canal, Ushering in New Era for the Segment and Global LNG Trade. Press Releases*. Autoridad del Canal de Panamá, 2016. Accessed in: 9th February 2017. Available at: <<https://micanaldepanama.com/expansion/2016/07/first-ever-lng-vessel-transits-the-expanded-panama-canal-ushering-in-new-era-for-the-segment-and-global-lng-trade/>>.
- ALVAREZ, E.; RUBIO, R.; RICALDE, H. Beach restoration with geotextile tubes as submerged breakwaters in Yucatan, Mexico. *Geotextiles and Geomembranes*, Elsevier, v. 25, n. 4, p. 233–241, 2007.
- AMANO, A.; IWAMOTO, N.; INOUE, T.; INOUCHI, Y. Seafloor environmental changes resulting from nineteenth century reclamation in Mishou Bay, Bungo channel, southwest Japan. *Environmental Geology*, v. 50, n. 7, p. 989–999, 2006. ISSN 1432-0495.
- BERTIN, X.; CHAUMILLON, E.; SOTTOLICHIO, A.; PEDREROS, R. Tidal inlet response to sediment infilling of the associated bay and possible implications of human activities: the Marennes-Oléron Bay and the Maumusson Inlet, France. *Continental Shelf Research*, v. 25, n. 9, p. 1115 – 1131, 2005. ISSN 0278-4343.
- BOLAM, S.; WHOMERSLEY, P. Development of macrofaunal communities on dredged material used for mudflat enhancement: a comparison of three beneficial use schemes after one year. *Marine Pollution Bulletin*, Elsevier, v. 50, n. 1, p. 40–47, 2005.
- BRASIL. *Federal Law N 8630/1993: "Lei dos Portos"*. Brasília, 1993. Available at: <http://www.planalto.gov.br/ccivil_03/leis/L8630.htm>.
- BRASIL. *Federal Law N 11610/2007: "Plano Nacional de Dragagem Postuária e Hidroviária"*. Brasília, 2007. Available at: <http://www.planalto.gov.br/ccivil_03/_ato2007-2010/2007/Lei/L11610.htm>
- BRASIL. *Federal Law N 12815/2013: "Plano Nacional de Dragagem Postuária e Hidroviária 2"*. Brasília, 2013. Available at: <http://www.planalto.gov.br/ccivil_03/_ato2011-2014/2013/lei/l12815.htm>
- BRASIL. *Programa Nacional de Dragagem - PND*. Secretaria de Portos da Presidência da República - SEP/PR, 2015. Accessed in: 7th February 2017. Disponível em: <<http://www.portosdobrasil.gov.br/assuntos1/pnd>>.
- BRUUN, P. Chapter 1 - development of tidal inlets. In: BRUUN, P. (Ed.). *Stability of Tidal Inlets: Theory and Engineering*. Elsevier, 1978, (Developments in Geotechnical Engineering,

v. 23). p. 13 – 38. 1978a. Available at:

<<http://www.sciencedirect.com/science/article/pii/B9780444417282500096>>

BRUUN, P. Chapter 2 - configuration of tidal inlets. In: BRUUN, P. (Ed.). *Stability of Tidal Inlets: Theory and Engineering*. Elsevier, 1978, (Developments in Geotechnical Engineering, v. 23). p. 39 – 82. 1978b. Available at:

<<http://www.sciencedirect.com/science/article/pii/B9780444417282500102>>

BRUUN, P.; GERRITSEN, F. Stability of coastal inlets. *Coastal Engineering Proceedings*, v. 1, n. 7, p. 23, 1960.

BTP. *Brasil Terminal Portuário inicia oficialmente as operações em seu*

moderno terminal no Porto de Santos. Brasil Terminal Portuário, 2013. Accessed in: 22nd February 2017. Available at:

<http://www.btp.com.br/brasilterminalportuarioiniciaoficialmenteasoperacoesemseumodernoterminalnoportodesantos/>

CHAUMILLON, E.; TESSIER, B.; WEBER, N.; TESSON, M.; BERTIN, X. Buried sandbodies within present-day estuaries (Atlantic coast of France) revealed by very high resolution seismic surveys. *Marine Geology*, v. 211, n. 3, p. 189 – 214, 2004. ISSN 0025-3227.

CHO, S.; JEON, B.; PARK, S.; YOON, H. Geotextile tube application as the cofferdam at the foreshore with large tidal range for Incheon Bridge project. *Geosynthetics in Civil and Environmental Engineering*, Springer, p. 591–596, 2009.

Chow, V.T. *Open-channel hydraulics*: New York, McGraw-Hill, 680 p, 1959.

CLEARY, W. J.; FITZGERALD, D. M. Tidal inlet response to natural sedimentation processes and dredging-induced tidal prism changes: Mason inlet, North Carolina. *Journal of Coastal Research*, JSTOR, p. 1018–1025, 2003.

CODESP. *Plano de Desenvolvimento e Zoneamento do Porto de Santos (PDZPS)*. Companhia de Docas do Estado de São Paulo, 2006.

CODESP. *Resumo Histórico*. Companhia de Docas do Estado de São Paulo, 2015. Accessed in: 11th January 2017. Available at: <<http://www.portodesantos.com.br/historia.php>>

COELHO, T. M. *Análise do transporte de sedimentos na região central da Baixada Santista (SP) através de modelagem numérica*. Tese (Doutorado) — Instituto Ocenográfico - Universidade de São Paulo, 2009.

- CORRÊA, T. B.; SOUZA, C. M. M. A.; GIRELI, T. Z. The influence of tidal prism on Port of Santos dredging. In: *Proceedings of Ninth International Conference on Coastal and Port Engineering in Developing Countries*. Rio de Janeiro, Brazil: PIANC, 2016.
- CORRÊA, T. B.; COSTA, J. H. O.; GIRELI, T. Z.; GARCIA, P. D. Evaluation of Proposed Jetties for Port of Santos Navigation Channel Depth Maintenance. In: *Proceedings of 34th PIANC-World Congress*. Panama City, Panama: PIANC, 2018.
- COURANT, R.; FRIEDRICHS, K.; LEWY, H. On the partial difference equations of mathematical physics. *IBM journal*, v. 11, n. 2, p. 215–234, 1967.
- CPEA. *Dredging regularion in Brazil: Management of contaminated sediments: Smart rivers* - Buenos Aires, Argentina, 2015. Available at: <http://www.cpeanet.com.br/wp-content/uploads/2016/10/Apresentacao_CPEA_PIANC.pdf>
- CUVILLIEZ, A.; DELOFFRE, J.; LAFITE, R.; BESSINETON, C. Morphological responses of an estuarine intertidal mudflat to constructions since 1978 to 2005: The Seine Estuary (France). *Geomorphology*, v. 104, n. 3, p. 165 – 174, 2009. ISSN 0169-555X.
- DAI, Z.; FAGHERAZZI, S.; MEI, X.; CHEN, J.; MENG, Y. Linking the infilling of the north branch in the Changjiang (Yangtze) estuary to anthropogenic activities from 1958 to 2013. *Marine Geology*, v. 379, p. 1 – 12, 2016. ISSN 0025-3227.
- DHI. *MIKE 21 & MIKE 3 Flow Model FM - Hydrodynamic and Transport Module, Scientific Documentation*. Copenhagen, Denmark, 2015. Danish Hydraulic Institute.
- DIECKMANN, R., OSTERHUN, M., PARTENSCKY, H.W. A comparison between German and North American tidal inlets. *Proceedings of the 21st International Conference on Coastal Engineering*, ASCE, 2681-2691. 1988.
- EMBRAPORT. *Um passo importante foi dado em 2009, com a entrada de dois grandes acionistas, ODEBRECHT TRANSPORT e a DUBAI PORTS WORLD*. EMBRAPORT - Empresa Brasileira de Terminais Portuários, 2013. Accessed in: 22nd February 2017. Available at: <<http://www.embraport.com/aembraport/historia/>>
- FEMAR. *Catálogo de estações maregráficas brasileiras*. Rio de Janeiro, 2000. Fundação de Estudos do Mar.
- FENG, L.; HE, J.; AI, J.; SUN, X.; BIAN, F.; ZHU, X. Evaluation for coastal reclamation feasibility using a comprehensive hydrodynamic framework: A case study in Haizhou Bay. *Marine Pollution Bulletin*, v. 100, n. 1, p. 182 – 190, 2015. ISSN 0025-326X.

FOWLER, J.; SPRAGUE, C. J.; TOUPS, D.; ENGLER, R. M. *Dredged material-filled geotextile containers*. [S.l.], 1995.

FRANCO, A. S. *Tides: Fundamentals, Analysis and Prediction*. 2. ed. São Paulo: Fundação Centro Tecnológico de Hidráulica (FCTH), 1988.

FRF. Capítulo 2: Histórico da atividade de dragagem no porto de Santos. In: *EIA - Dragagem de Aprofundamento do Canal de Navegação e Bacias de Evolução do Porto Organizado de Santos/SP*. Rio de Janeiro: Fundação Ricardo Franco, 2008.

FRF. Capítulo 7: Justificativas. In: *EIA - Dragagem de Aprofundamento do Canal de Navegação e Bacias de Evolução do Porto Organizado de Santos/SP*. Rio de Janeiro: Fundação Ricardo Franco, 2008.

FRIEDRICHS, C. T. Stability shear stress and equilibrium cross-sectional geometry of sheltered tidal channels. *Journal of Coastal Research*, JSTOR, p. 1062–1074, 1995.

GARCIA, P. D.; ARAÚJO, R. N.; SILVA, G. d. C.; BAPTISTELLI, S. C.; ALFREDINI, P. Preparo de bases batimétricas, de agitação e circulação para o litoral do estado de São Paulo. *Boletim Técnico da Escola Politécnica da USP. BT/PMI, Escola Politécnica da USP*, v. 1, n. 105, p. 1–56, 2002.

GONG, W.; SHEN, J.; JIA, J. Feedback between tidal hydrodynamics and morphological changes induced by natural process and human interventions in a wave-dominated tidal inlet: Xiaohai, Hainan, China. *Acta Oceanologica Sinica*, v. 28, n. 3, p. 93–113, 2009.

GUNNEWIEK, A.F.K.; GIRELI, T.Z.; GARCIA, P.D. Metodologia para obtenção de dados de maré utilizando superfícies baseadas em modelagem numérica. In: XXII SBRH – Sipiósio Brasileiro de Recursos Hídricos. Florianópolis, Brazil. 2017.

HARARI, J. *Fundamentos de modelagem numérica em Oceanografia*. 1. ed. São Paulo: SALT | Sea and Limno Technology, 2015.

HARARI, J.; CAMARGO, R. Modelagem numérica da região costeira de Santos (SP): circulação de maré. *Revista Brasileira de Oceanografia*, SciELO Brasil, v. 46, n. 2, p. 135–156, 1998.

HARARI, J.; CAMARGO, R. de. Simulação da propagação das nove principais componentes de maré na plataforma sudeste brasileira através de modelo numérico hidrodinâmico. *Boletim do Instituto Oceanográfico*, v. 42, n. 1-2, p. 35–54, 1994.

HARARI, J.; CAMARGO, R. de. Numerical simulation of the tidal propagation in the coastal region of Santos (Brazil, 24 s 46 w). *Continental Shelf Research*, Elsevier, v. 23, n. 16, p. 1597–1613, 2003.

- HILSDORF, W. d. C.; NETO, N.; SOUZA, M. de. Port of Santos: prospection on the causes of access difficulties. *Gestão & Produção*, SciELO Brasil, v. 23, n. 1, p. 219–231, 2016.
- HUGHES, S. A. Equilibrium cross sectional area at tidal inlets. *Journal of Coastal Research*, JSTOR, p. 160–174, 2002.
- HUME, T. M. AND HERDENDORF, C. E. A geomorphic classification of estuaries and its application to coastal resource management – A New Zealand example. *Journal of Ocean and Shoreline Management*, 11, 249-274. 1988.
- HUME, T. M. AND HERDENDORF, C. E. On the use of empirical stability relationships for characterising estuaries. *Journal of Coastal Research*, JSTOR, p. 413–422, 1993.
- INPH. *Relatório INPH no 018 / 2007 - Projeto Geométrico da Infra-Estrutura Aquaviária ao Porto de Santos - SP - Anexo XI*. Rio de Janeiro, 2007.
- IPEA. *Texto para Discussão 1408: Portos brasileiros 2009: Ranking, área de influência, porte e valor agregado médio dos produtos movimentados*. Rio de Janeiro, 2009. Available at: <http://www.ipea.gov.br/portal/images/stories/PDFs/TDs/td_1408.pdf>
- JARRETT, J. T. *Tidal prism-inlet area relationships*. GITI report no. 3. Coastal Engineering Research Center, US Army Corps of Engineers, Fort Belvoir, VA., 1976.
- LEE, E.; DOUGLAS, R. Geotextile tubes as submerged dykes for shoreline management in Malaysia. *Geotextiles and Geomembranes*, Elsevier, v. 30, p. 8–15, 2012.
- LEITÃO, J. C.; MATEUS, M.; NEVES, R. *Calibration of the hydrodynamic model for the Santos Estuary*. Technical Report, 2008.
- LIRIA, P.; GAREL, E.; URIARTE, A. The effects of dredging operations on the hydrodynamics of an ebb tidal delta: Oka estuary, northern Spain. *Continental Shelf Research*, v. 29, n. 16, p. 1983 – 1994, 2009. ISSN 0278-4343. Special issue in honour of Michael Collins.
- LIU, Y.; WANG, Y. P.; LI, Y.; GAO, J.; JIA, J.; XIA, X.; GAO, S. Coastal embayment long-term erosion/siltation associated with p-a relationships: A case study from Jiaozhou Bay, China. *Journal of Coastal Research*, The Coastal Education and Research Foundation 1656 Cypress Row Drive, West Palm Beach, FL 33411, USA, v. 28, n. 5, p. 1236–1246, 2012.
- MALHADAS, M. S.; SILVA, A.; LEITÃO, P. C.; NEVES, R. Effect of the bathymetric changes on the hydrodynamic and residence time in Óbidos Lagoon (Portugal). *Journal of Coastal Research*, JSTOR, p. 549–553, 2009.

MARMIL. *Centro de Hidrografia da Marinha*. Marinha do Brasil, 2015. Accessed in: 30th September 2015. Available at: <http://www.mar.mil.br/dhn/chm/box-cartas-raster/raster_disponiveis.html>

MEHTA, A.; ÖZSOY, E. Chapter 3 - inlet hydraulics: 3.1 flow dynamics and nearshore transport. In: BRUUN, P. (Ed.). *Stability of Tidal Inlets: Theory and Engineering*. Elsevier, 1978, (Developments in Geotechnical Engineering, v. 23). p. 83 – 161. Available at: <<http://www.sciencedirect.com/science/article/pii/B9780444417282500114>>

MKR. Volume I: Capítulos 1 a 7. In: *EIA - Terminal Portuário EMBRAPORT*. [S.l.]: EMBRAPORT - Empresa Brasileira de Terminais Portuários, 2003.

MKR. *RIMA - Brasil Terminal Portuário*: Relatório de impacto ambiental. São Paulo, 2008.

MOURA, D. Between the Atlantic and the coast: confluence of trade routes in a peripheral port of Portuguese America (Santos, 1808-1822). *Tempo*, SciELO Brasil, v. 19, n. 34, p. 95–116, 2013.

NICHOLS, M. M.; HOWARD-STROBEL, M. M. Evolution of an urban estuarine harbor: Norfolk, Virginia. *Journal of Coastal Research*, JSTOR, p. 745–757, 1991.

O'BRIEN, M. P. Equilibrium flow areas of inlets on sandy coasts. *Journal of the Waterways and Harbors Division*, ASCE, p. 43–52, 1969.

OH, Y. I.; SHIN, E. C. Using submerged geotextile tubes in the protection of the e. Korean shore. *Coastal Engineering*, Elsevier, v. 53, n. 11, p. 879–895, 2006.

OLIVEIRA, A.; FORTUNATO, A. B.; REGO, J. R. Effect of morphological changes on the hydrodynamics and flushing properties of the Óbidos Lagoon (Portugal). *Continental Shelf Research*, v. 26, n. 8, p. 917 – 942, 2006. ISSN 0278-4343.

OOST, A. Sedimentological implications of morphodynamic changes in the ebb-tidal delta, the inlet and the drainage basin of the Zoutkamperlaag tidal inlet (Dutch Wadden Sea), induced by a sudden decrease in the tidal prism. In: Flemming, BW and Bartholoma, A (Ed.). *TIDAL SIGNATURES IN MODERN AND ANCIENT SEDIMENTS*. OSNEY MEAD, OXFORD, ENGLAND OX2 0EL: BLACKWELL SCIENCE PUBL, 1995. (INTERNATIONAL ASSOCIATION OF SEDIMENTOLOGISTS SPECIAL PUBLICATION, 24), p. 101–119. ISBN 0-86542-978-2. 3rd International Research Symposium/6th International Senckenberg Conference - Modern and Ancient Clastic Tidal Deposits (TIDAL CLASTICS 92), WILHELMSHAVEN, GERMANY, AUG 25-28, 1992.

PICADO, A.; DIAS, J. M.; FORTUNATO, A. B. Tidal changes in estuarine systems induced by local geomorphologic modifications. *Continental Shelf Research*, v. 30, n. 17, p. 1854 – 1864, 2010. ISSN 0278-4343.

POWELL, M. A.; THIEKE, R. J.; MEHTA, A. J. Morphodynamic relationships for ebb and flood delta volumes at Florida's tidal entrances. *Ocean Dynamics*, Springer, v. 56, n. 3-4, p. 295–307, 2006.

ROVERSI, F. *Estudo hidrodinâmico e de renovação das águas do sistema estuarino de Santos*. 2012. Tese (Doutorado) — Dissertação (Mestrado)-Instituto Alberto Luiz Coimbra de Pós-Graduação e Pesquisa de Engenharia, Universidade Federal do Rio de Janeiro, Rio de Janeiro, 2012.

ROVERSI, F.; ROSMAN, P.; HARARI, J. Análise das trajetórias das águas continentais afluentes ao sistema estuarino de Santos. *Revista Brasileira de Recursos Hídricos*, v. 21, n. 1, p. 242–250, 2016.

SANTOS BRASIL. *TECON SANTOS*. SANTOS BRASIL, 2011. Accessed in: 8th February 2017. Available at: <<http://www.mediagroup.com.br/HOST/SantosBrasil/2011/port/ra/04.htm>>

SCAZUFCA, M. *A primazia do Porto de Santos no cenário portuário nacional no período contemporâneo. Determinantes logísticos, territoriais e de gestão*. Tese (Doutorado) — Universidade de São Paulo, 2012.

SHEEHAN, C.; HARRINGTON, J. An environmental and economic analysis for geotube coastal structures retaining dredge material. *Resources, Conservation and Recycling*, Elsevier, v. 61, p. 91–102, 2012.

SHI, J.; LI, G.; WANG, P. Anthropogenic influences on the tidal prism and water exchanges in Jiaozhou bay, Qingdao, china. *Journal of Coastal Research*, The Coastal Education and Research Foundation 1656 Cypress Row Drive, West Palm Beach, FL 33411, USA, v. 27, n. 1, p. 57–72, 2011.

SHIN, E.; OH, Y. Coastal erosion prevention by geotextile tube technology. *Geotextiles and Geomembranes*, Elsevier, v. 25, n. 4, p. 264–277, 2007.

SONDOTÉCNICA. *Comportamento Hidráulico e Sedimentológico do Estuário Santista*. [S.l.], 1977a. Relatório Final- Texto.

SONDOTÉCNICA. *Comportamento Hidráulico e Sedimentológico do Estuário Santista*. [S.l.], 1977b. Relatório Final- Desenhos.

SOUZA, M. M. A. *Comparação de modelos numéricos bidimensional e tridimensional para a avaliação de mudanças ambientais, aplicado à região costeira de Santos*. Tese (Doutorado) — Faculdade de Engenharia Civil, Arquitetura e Urbanismo – Universidade Estadual de Campinas, 2017.

- STIVE, M.; JI, L.; BROUWER, R. L.; KREEKE, C. van de; RANASINGHE, R. Empirical relationship between inlet cross-sectional area and tidal prism: A re-evaluation. *Coastal Engineering Proceedings*, v. 1, n. 32, p. 86, 2011.
- TOWNEND, I. An examination of empirical stability relationships for UK estuaries. *Journal of Coastal Research*, v. 21, n. 5, p. 1042–1053, 2005.
- TRIBUNA, A. *Cetesb atesta recuperação definitiva da área da BTP*. A Tribuna, 2015. Accessed in: 8th March 2017. Available at: <<http://www.atribuna.com.br/noticias/detalhe/noticia/cetesb-atesta-recuperacao-definitiva-da-area-da-btp/?cHash=d654e4924a2ffe2a1b469838fe7deadf>>
- UNISANTOS; CETESB; CODESP. *Agenda Ambiental do Porto de Santos*. Santos, 2014. Available at: <http://189.50.187.200/pdfjs/web/viewer.html?file=/down/meio_ambiente/agenda-ambiental.pdf?13042016>
- URS. Chapter 3: Project description. In: *Environmental Impact Study - Panama Canal Expansion - Third Set of Locks Project*. [S.l.]: URS Holdings, Inc., 2007
- VAN DE KREEKE, J. Can multiple tidal inlets be stable? *Estuarine, Coastal and Shelf Science*, v. 30, n. 3, p. 261 – 273, 1990. ISSN 0272-7714.
- VAN DE KREEKE, J. Stability analysis of a two-inlet bay system. *Coastal Engineering*, v. 14, n. 6, p. 481 – 497, 1990. ISSN 0378-3839.
- VAN DE KREEKE, J. Equilibrium and cross-sectional stability of tidal inlets: application to the Frisian Inlet before and after basin reduction. *Coastal Engineering*, v. 51, n. 5–6, p. 337 – 350, 2004. ISSN 0378-3839.
- VAN DER WAL, D.; PYE, K.; NEAL, A. Long-term morphological change in the Ribble estuary, northwest England. *Marine Geology*, v. 189, n. 3, p. 249 – 266, 2002. ISSN 0025-3227.
- WANG, J.; HONG, H.; ZHOU, L.; HU, J.; JIANG, Y. Numerical modeling of hydrodynamic changes due to coastal reclamation projects in Xiamen bay, China. *Chinese Journal of Oceanology and Limnology*, v. 31, n. 2, p. 334–344, 2013. ISSN 1993-5005.
- WANG, Y. P.; GAO, S.; JIA, J.; LIU, Y.; GAO, J. Remarkable morphological change in a large tidal inlet with low sediment-supply. *Continental Shelf Research*, v. 90, p. 79 – 95, 2014. ISSN 0278-4343. Sediment Dynamics and Related Biogeochemical Effects in the Eastern China Shelf Seas.

WARNER, J. C.; GEYER, W. R.; LERCZAK, J. A. Numerical modeling of an estuary: A comprehensive skill assessment. *Journal of Geophysical Research: Oceans*, Wiley Online Library, v. 110, n. C5, 2005.

WEDA. *WEDA 2013 Environmental Dredging Award: EMBRAPORT container and bulk terminal - Santos, Brazil*. [S.l.], 2013. Available at: <<https://www.westerndredging.org/phocadownload/2013EnvironmentalAwards/weda%202013%20embraport%20application.pdf>>

WILLIAMS, J. R.; DELLAPENNA, T. M.; LEE, G. Shifts in depositional environments as a natural response to anthropogenic alterations: Nakdong estuary, South Korea. *Marine Geology*, v. 343, p. 47 – 61, 2013. ISSN 0025-3227.

WILLMOTT, C. J. On the validation of models. *Physical geography*, Taylor & Francis, v. 2, n. 2, p. 184–194, 1981.

YOZZO, D. J.; WILBER, P.; WILL, R. J. Beneficial use of dredged material for habitat creation, enhancement, and restoration in New York–New Jersey harbor. *Journal of Environmental Management*, Elsevier, v. 73, n. 1, p. 39–52, 2004.

I. APPENDIX

I.1. Santos estuary inlet Tidal Prism computation and cross-sectional area estimates based on coefficients $C=1.65 \times 10^{-3}$ and $q=0.81$

#	Scenario A		Scenario B		Scenario C		Scenario D	
	Tidal Prism (m ³)	Area (m ²)	Tidal Prism (m ³)	Area (m ²)	Tidal Prism (m ³)	Area (m ²)	Tidal Prism (m ³)	Area (m ²)
	5.51E+07	6,132	5.34E+07	5,977	5.53E+07	6,175	5.36E+07	6,021
	ΔP	ΔA						
1	220,825	35.17	214,698	34.38	216,558	34.62	209,735	33.73
2	312,067	46.54	304,965	45.68	304,958	45.68	294,922	44.46
3	411,911	58.27	400,176	56.93	393,296	56.13	380,615	54.66
4	598,475	78.87	585,041	77.43	583,994	77.32	566,322	75.42
5	768,597	96.58	750,656	94.75	744,106	94.08	722,014	91.81
6	938,719	113.56	916,271	111.36	904,219	110.17	877,707	107.55
7	1,108,841	129.97	1,081,886	127.40	1,064,331	125.72	1,033,399	122.76
8	1,278,963	145.89	1,247,501	142.98	1,224,443	140.84	1,189,092	137.53
9	1,448,055	161.33	1,411,957	158.07	1,383,431	155.47	1,343,347	151.82
10	1,615,245	176.26	1,574,273	172.63	1,540,343	169.61	1,494,949	165.55
11	1,757,333	188.72	1,710,229	184.61	1,665,484	180.69	1,615,959	176.32
12	1,881,449	199.44	1,827,313	194.78	1,767,881	189.64	1,715,068	185.03
13	2,005,566	210.04	1,944,398	204.83	1,870,278	198.49	1,814,177	193.65
14	2,087,820	216.99	2,022,614	211.48	1,941,608	204.59	1,882,789	199.56
15	2,093,488	217.46	2,029,404	212.06	1,959,255	206.10	1,898,935	200.94
16	2,098,699	217.90	2,035,784	212.60	1,976,805	207.59	1,914,979	202.32
17	2,103,909	218.34	2,042,165	213.14	1,994,354	209.09	1,931,023	203.69
18	2,096,200	217.69	2,034,609	212.50	1,998,903	209.47	1,934,613	204.00
19	2,065,407	215.10	2,002,151	209.75	1,980,221	207.88	1,915,949	202.40
20	2,034,614	212.50	1,969,692	206.99	1,961,539	206.29	1,897,286	200.80
21	2,003,821	209.89	1,937,234	204.22	1,942,857	204.70	1,878,622	199.20
22	1,973,028	207.27	1,904,776	201.45	1,924,175	203.11	1,859,958	197.60
23	1,912,980	202.15	1,845,056	196.31	1,880,921	199.40	1,818,017	193.98
24	1,842,437	196.09	1,775,782	190.32	1,829,656	194.99	1,768,537	189.69
25	1,771,893	189.98	1,706,508	184.29	1,778,391	190.55	1,719,057	185.38
26	1,701,350	183.83	1,637,234	178.20	1,727,125	186.09	1,669,576	181.05
27	1,630,040	177.57	1,567,302	172.01	1,674,920	181.52	1,619,196	176.61
28	1,540,661	169.64	1,481,874	164.38	1,600,537	174.96	1,547,592	170.26
29	1,451,282	161.62	1,396,446	156.66	1,526,155	168.34	1,475,988	163.85
30	1,361,903	153.51	1,311,018	148.85	1,451,772	161.67	1,404,383	157.38
31	1,272,523	145.30	1,225,590	140.94	1,377,390	154.92	1,332,779	150.85
32	1,183,803	137.04	1,140,857	133.00	1,303,841	148.19	1,261,982	144.32
33	1,093,247	128.48	1,054,617	124.79	1,227,062	141.08	1,188,244	137.45
34	988,485	118.42	954,536	115.11	1,120,976	131.12	1,086,669	127.86
35	884,370	108.21	854,990	105.29	1,015,503	121.03	985,470	118.12
36	780,256	97.77	755,444	95.24	910,031	110.74	884,271	108.20

#	Scenario A		Scenario B		Scenario C		Scenario D	
	Tidal Prism (m ³)	Area (m ²)	Tidal Prism (m ³)	Area (m ²)	Tidal Prism (m ³)	Area (m ²)	Tidal Prism (m ³)	Area (m ²)
	5.51E+07	6,132	5.34E+07	5,977	5.53E+07	6,175	5.36E+07	6,021
	ΔP	ΔA						
37	676,141	87.06	655,898	84.94	804,558	100.23	783,073	98.05
38	572,026	76.03	556,353	74.34	699,086	89.44	681,874	87.66
39	467,911	64.61	456,807	63.37	593,613	78.35	580,675	76.96
40	380,365	54.63	372,441	53.71	495,191	67.65	485,723	66.60
41	302,764	45.41	297,188	44.73	401,002	57.02	394,521	56.27
42	225,164	35.73	221,935	35.31	306,812	45.90	303,318	45.48
43	147,563	25.37	146,681	25.25	212,622	34.11	212,116	34.04

I.2. Santos estuary inlet Tidal Prism computation and cross-sectional area estimates based on JARRETT (1976), HUGHES (2002) and HUME AND HERDENDORF (1993) coefficients

#	Tidal Prism (m ³)	Jarrett (1976) - All Inlets	Hughes (2002)	Hume and Herdendorf (1993) - River mouth (New Zealand)
	5.36E+07	Area (m ²)	Area (m ²)	Area (m ²)
#	ΔP	ΔA	ΔA	ΔA
1	209,735	21.44	31.49	46.88
2	294,922	29.43	42.65	60.68
3	380,615	37.31	53.53	73.60
4	566,322	54.00	76.23	99.43
5	722,014	67.68	94.63	119.50
6	877,707	81.16	112.59	138.54
7	1,033,399	94.47	130.20	156.77
8	1,189,092	107.64	147.53	174.34
9	1,343,347	120.57	164.44	191.21
10	1,494,949	133.17	180.86	207.33
11	1,615,959	143.17	193.83	219.91
12	1,715,068	151.32	204.38	230.05
13	1,814,177	159.44	214.86	240.04
14	1,882,789	165.04	222.08	246.88
15	1,898,935	166.35	223.77	248.48
16	1,914,979	167.66	225.45	250.07
17	1,931,023	168.97	227.13	251.66
18	1,934,613	169.26	227.51	252.01
19	1,915,949	167.74	225.55	250.17
20	1,897,286	166.22	223.60	248.32
21	1,878,622	164.70	221.64	246.47
22	1,859,958	163.18	219.68	244.61
23	1,818,017	159.75	215.26	240.43
24	1,768,537	155.70	210.04	235.46
25	1,719,057	151.65	204.80	230.45
26	1,669,576	147.58	199.55	225.41
27	1,619,196	143.44	194.18	220.24
28	1,547,592	137.53	186.52	212.83
29	1,475,988	131.60	178.82	205.33
30	1,404,383	125.65	171.08	197.75
31	1,332,779	119.69	163.29	190.07
32	1,261,982	113.76	155.55	182.37
33	1,188,244	107.57	147.43	174.25
34	1,086,669	98.99	136.16	162.85
35	985,470	90.39	124.82	151.24
36	884,271	81.72	113.34	139.33

	Tidal Prism (m ³)	Jarrett (1976) - All Inlets	Hughes (2002)	Hume and Herdendorf (1993) - River mouth (New Zealand)
		Area (m ²)	Area (m ²)	Area (m ²)
	5.36E+07	4,795	6,531	7,581
#	ΔP	ΔA	ΔA	ΔA
37	783,073	72.99	101.72	127.08
38	681,874	64.17	89.93	114.44
39	580,675	55.27	77.95	101.34
40	485,723	46.81	66.50	88.52
41	394,521	38.58	55.26	75.63
42	303,318	30.21	43.73	61.98
43	212,116	21.66	31.81	47.28

II. ANNEX

II.1. Checklist of features that characterize each estuary type (Hume and Herdendorf, 1988)

Checklist – Estuary types (Hume and Herdendorf (1988))
Fluvial Erosion
<i>Type 1. Funnel-shaped</i>
1. Inlet flares, unrestricted by spit or rock barrier
2. No tidal gorge
3. Large inlet width to mean width ratio
4. Low freshwater inflow cf. tidal prism
5. Tide-dominated hydrology
6. Extensive intertidal areas
<i>Type 2. Headland enclosed</i>
1. Rock headland constricted inlet
2. Inlet gorge deep and stable
3. Numerous tidal creeks branching of the embayment
4. Large shoreline length to inlet width ratio
5. Low freshwater inflow
6. Tide dominated hydrology
7. Well mixed except in headwaters
<i>Barrier enclosed</i>
<i>Type 3. Double-spit</i>
<i>Type 4. Single-spit</i>
<i>Type 5. Tombolo</i>
<i>Type 6. Island</i>
1. Spit(s), tombolo or island Holocene sedimentary barrier forms enclosure
2. Unstable inlet, narrow gorge, with flood and ebb tide shoals
3. Extensive intertidal area
4. Small inlet width to mean width ratio
5. Low freshwater inflow
6. Tide dominated hydrology
7. Well mixed, except in headwaters
<i>Type 7. Beach</i>
1. Small estuaries that have intermittent connection with the sea
2. Low freshwater inflow, small catchments
3. Inlet restricted by a barrier beach
4. Direct exchange with the ocean only near high tide
<i>River mouth</i>
1. Large catchment to estuary area ratio
2. River flow prohibits formation of flood tide shoal
3. Large freshwater inflow
4. River dominated hydrology
<i>Type 8. Straight-banked</i>
5. Parallel or funnel-shaped entrances
6. Mark salinity structure
<i>Type 9. Spit-lagoon</i>
5. Estuary formed by barrier spit enclosure
6. Marked salinity structure
<i>Type 10. Spit-lagoon 2</i>
5. Barrier spit enclosure
6. No tidal prism, tide produces backwater effect on flows in estuary

Checklist – Estuary types (Hume and Herdendorf (1988))
<i>Type 11. Deltaic</i>
5. Numerous channel distributaries at mouth
6. Seawater only enters at time of very low river flows
Marine/fluvial erosion
<i>Type 12. Coastal Embayment</i>
1. Wide, stable inlet, partial enclosure
2. Rock bounded, arcuate enclosure
3. Small catchment to estuary area ratio
4. Intertidal area small; cove beaches
5. Freshwater inflow small
6. Inlet width to mean estuary width ≤ 1
Tectonism
<i>Type 13. Fault defined embayment</i>
1. Parallel shores, structurally defined
2. Rectangular embayment with wide deep rocky inlet
3. Inlet width < 2 km
4. Well mixed
<i>Type 14. Diastrophic embayment</i>
1. Inlet width > 5 km
2. Well mixed
Volcanism
<i>Type 15. Volcanic embayment</i>
1. Circular in plan, defined by crater rim
2. Very small catchment
3. Little freshwater inflow
4. Tide dominated hydrology
5. Narrow inlet
Glaciation
<i>Type 16. Glacial embayment</i>
1. Parallel shores, elongate
2. Rock bounded throat
3. Very deep
4. Marked salinity structure

II.2. Manning's n for Channels (Chow, 1959)

Type of Channel and Description	Minimum	Normal	Maximum
Natural streams - minor streams (top width at floodstage < 100 ft)			
1. Main Channels			
a. clean, straight, full stage, no rifts or deep pools	0.025	0.03	0.033
b. same as above, but more stones and weeds	0.03	0.035	0.04
c. clean, winding, some pools and shoals	0.033	0.04	0.045
d. same as above, but some weeds and stones	0.035	0.045	0.05
e. same as above, lower stages, more ineffective slopes and sections	0.04	0.048	0.055
f. same as "d" with more stones	0.045	0.05	0.06
g. sluggish reaches, weedy, deep pools	0.05	0.07	0.08
h. very weedy reaches, deep pools, or floodways with heavy stand of timber and underbrush	0.075	0.1	0.15

Type of Channel and Description	Minimum	Normal	Maximum
2. Mountain streams, no vegetation in channel, banks usually steep, trees and brush along banks submerged at high stages			
a. bottom: gravels, cobbles, and few boulders	0.03	0.04	0.05
b. bottom: cobbles with large boulders	0.04	0.05	0.07
3. Floodplains			
a. Pasture, no brush			
1. short grass	0.025	0.03	0.035
2. high grass	0.03	0.035	0.05
b. Cultivated areas			
1. no crop	0.02	0.03	0.04
2. mature row crops	0.025	0.035	0.045
3. mature field crops	0.03	0.04	0.05
c. Brush			
1. scattered brush, heavy weeds	0.035	0.05	0.07
2. light brush and trees, in winter	0.035	0.05	0.06
3. light brush and trees, in summer	0.04	0.06	0.08
4. medium to dense brush, in winter	0.045	0.07	0.11
5. medium to dense brush, in summer	0.07	0.1	0.16
d. Trees			
1. dense willows, summer, straight	0.11	0.15	0.2
2. cleared land with tree stumps, no sprouts	0.03	0.04	0.05
3. same as above, but with heavy growth of sprouts	0.05	0.06	0.08
4. heavy stand of timber, a few down trees, little undergrowth, flood stage below branches	0.08	0.1	0.12
5. same as 4. with flood stage reaching branches	0.1	0.12	0.16
4. Excavated or Dredged Channels			
a. Earth, straight, and uniform			
1. clean, recently completed	0.016	0.018	0.02
2. clean, after weathering	0.018	0.022	0.025
3. gravel, uniform section, clean	0.022	0.025	0.03
4. with short grass, few weeds	0.022	0.027	0.033
b. Earth winding and sluggish			
1. no vegetation	0.023	0.025	0.03
2. grass, some weeds	0.025	0.03	0.033
3. dense weeds or aquatic plants in deep channels	0.03	0.035	0.04
4. earth bottom and rubble sides	0.028	0.03	0.035
5. stony bottom and weedy banks	0.025	0.035	0.04
6. cobble bottom and clean sides	0.03	0.04	0.05
c. Dragline-excavated or dredged			
1. no vegetation	0.025	0.028	0.033
2. light brush on banks	0.035	0.05	0.06
d. Rock cuts			

Type of Channel and Description	Minimum	Normal	Maximum
1. smooth and uniform	0.025	0.035	0.04
2. jagged and irregular	0.035	0.04	0.05
e. Channels not maintained, weeds and brush uncut			
1. dense weeds, high as flow depth	0.05	0.08	0.12
2. clean bottom, brush on sides	0.04	0.05	0.08
3. same as above, highest stage of flow	0.045	0.07	0.11
4. dense brush, high stage	0.08	0.1	0.14
5. Lined or Constructed Channels			
a. Cement			
1. neat surface	0.01	0.011	0.013
2. mortar	0.011	0.013	0.015
b. Wood			
1. planed, untreated	0.01	0.012	0.014
2. planed, creosoted	0.011	0.012	0.015
3. unplaned	0.011	0.013	0.015
4. plank with battens	0.012	0.015	0.018
5. lined with roofing paper	0.01	0.014	0.017
c. Concrete			
1. trowel finish	0.011	0.013	0.015
2. float finish	0.013	0.015	0.016
3. finished, with gravel on bottom	0.015	0.017	0.02
4. unfinished	0.014	0.017	0.02
5. gunite, good section	0.016	0.019	0.023
6. gunite, wavy section	0.018	0.022	0.025
7. on good excavated rock	0.017	0.02	
8. on irregular excavated rock	0.022	0.027	
d. Concrete bottom float finish with sides of:			
1. dressed stone in mortar	0.015	0.017	0.02
2. random stone in mortar	0.017	0.02	0.024
3. cement rubble masonry, plastered	0.016	0.02	0.024
4. cement rubble masonry	0.02	0.025	0.03
5. dry rubble or riprap	0.02	0.03	0.035
e. Gravel bottom with sides of:			
1. formed concrete	0.017	0.02	0.025
2. random stone mortar	0.02	0.023	0.026
3. dry rubble or riprap	0.023	0.033	0.036
f. Brick			
1. glazed	0.011	0.013	0.015
2. in cement mortar	0.012	0.015	0.018
g. Masonry			
1. cemented rubble	0.017	0.025	0.03
2. dry rubble	0.023	0.032	0.035
h. Dressed ashlar/stone paving	0.013	0.015	0.017
i. Asphalt			

Type of Channel and Description	Minimum	Normal	Maximum
1. smooth	0.013	0.013	
2. rough	0.016	0.016	
j. Vegetal lining	0.03		0.5